p63 is a key regulator of iRHOM2 signalling in the keratinocyte stress response

Paola Arcidiacono[1], Catherine M. Webb[1], Matthew A. Brooke[1], Huiqing Zhou[2,3], Paul J. Delaney[1], Keat-Eng Ng[1], Diana C. Blaydon[1], Andrew Tinker[4], David P. Kelsell[1*] and Anissa Chikh[1*]

[1] Blizard Institute, Barts and the London School of Medicine and Dentistry, Queen Mary University of London, London E1 2AT, UK

[2] Department of Human Genetics, Nijmegen Centre for Molecular Life Sciences, Radboud University Nijmegen Medical Centre, Nijmegen, The Netherlands

[3] Department of Molecular Developmental Biology, Radboud University, Nijmegen, The Netherlands

[4] The Heart Centre, William Harvey Research Institute, Barts and the London School of Medicine and Dentistry, Queen Mary University of London, Charterhouse Square, London EC1M 6BQ, UK

[*] joint senior authors.

Correspondence to David Kelsell: d.p.kelsell@qmul.ac.uk ; or Anissa Chikh: a.chikh@qmul.ac.uk

Abstract

Hyperproliferative keratinocytes induced by trauma, hyperkeratosis and/or inflammation display molecular signatures similar to those of palmoplantar epidermis. Inherited gain-of-function mutations in RHBDF2 (encoding iRHOM2) are associated with a hyperproliferative palmoplantar keratoderma and squamous oesophageal cancer syndrome (termed TOC). In contrast, genetic ablation of *rhbdf2* in mice leads to a thinning of the mammalian footpad, and reduces keratinocyte hyperproliferation and migration. Here, we report that iRHOM2 is a novel target gene of p63 and that both p63 and iRHOM2 differentially regulate cellular stress-associated signalling pathways in normal and hyperproliferative keratinocytes. We demonstrate that p63-iRHOM2 regulates cell survival and response to oxidative stress via modulation of SURVIVINandCytoglobin, respectively. Furthermore, the antioxidant compound Sulforaphane downregulates p63-iRHOM2 expression, leading to reduced proliferation, inflammation, survival and ROS production. These findings elucidate a novel

34 p63 associated pathway that identifies iRHOM2 modulation as a potential therapeutic target
35 to treat hyperproliferative skin disease and neoplasia.

36 **Introduction**

37

38 Keratinocyte hyperproliferation and inflammation are common to many skin disorders, from
39 the more prevalent conditions such as psoriasis and atopic eczema to the rarer monogenic
40 skin diseases which include the palmoplantar keratodermas (PPKs). The PPKs are
41 characterised by different patterns of hyperproliferative thickening of the palms and soles,
42 which are often painful [1,2]. Furthermore, PPK can also be associated with non-cutaneous
43 conditions such as hearing loss, cardiomyopathy and oesophageal cancer [3,4]. For example,
44 inherited dominant mutations in RHBDF2, the gene encoding iRHOM2, are the genetic basis
45 of the inherited syndrome Tylosis (Palmoplantar keratoderma, PPK) with Oesophageal
46 Cancer (TOC, OMIM: 148500) [5].

47

48 iRHOM2 is an inactive member of the seven transmembrane family of Rhomboid serine
49 proteases [6]. iRHOM2 can control activation and trafficking of ADAM17 (also known as TACE;
50 TNFα converting enzyme) from endoplasmic reticulum to the Golgi and then to the cell
51 surface [7-10]. ADAM17 is a membrane-anchored metalloprotease with a wide range of
52 substrates including cytokines (TNFα, IL-6), many receptors (IL-6R, TNF-R), growth factors
53 (TGFα, AREG) and adhesion proteins [11]. The autosomal dominant TOC-associated missense
54 mutations, located in the highly conserved cytoplasmic amino-terminal domain of iRHOM2,
55 lead to increased ADAM17 activity and the "shedding" of its associated substrates at the cell
56 surface [9]. TOC keratinocytes have constitutively high levels of, for example, TGFα, AREG, IL-
57 6R and IL-6. Thus, TOC-associated iRHOM2 mutations promote cell growth and migration in
58 keratinocytes, exhibiting similar features to the inflammatory skin disease psoriasis,
59 epithelial cancer cell lines and have a constitutive wound healing phenotype [5,12].

60

61 We have recently described [12] an important role for iRHOM2 in the regulation of the
62 epithelial response to physical stress by identifying Keratin 16 (K16) as a novel interacting
63 binding partner. TOC-associated iRHOM2 alters the dynamics of K16 regulation, including
64 the hetero-dimerisation with its type II binding partner K6. *In vitro* depletion of iRHOM2 in

65 TOC keratinocytes reduced K16 expression, proliferation and inflammation signalling. In
66 contrast to the hyperproliferative TOC palmoplantar epidermis, *irhom2*$^{-/-}$ mice have a much
67 thinner footpad epidermis compared to control mice. This striking cutaneous phenotype is
68 associated with loss of K16 expression.
69
70 In this study we showed different signalling mechanisms between normal interfollicular and
71 palmoplantar epidermis. The stressed palmoplantar epidermis mirrors disorders of
72 keratinocyte hyperproliferation. To date, no studies have investigated the transcriptional
73 regulation of iRHOM2. Here, we demonstrate that iRHOM2 is a direct molecular target of
74 the transcription factor p63, the "master regulator" of epithelial development [13,14].
75 Alteration of p63 expression is observed in oesophageal cancer, not only in carcinomas, but
76 also in dysplasia [15,16]. *TP63* is expressed as multiple isoforms from alternative promoters
77 with the N-terminal transactivation (TA) domain or dominant-negative (ΔN) and, in addition,
78 these TAp63 and ΔNp63 transcripts can be alternatively spliced at the C-terminus to
79 generate proteins designated α, β, and γ [13]. The ΔNp63α isoform of p63 is expressed at high
80 levels in the proliferative basal layer of the epidermis, suggesting the important role for this
81 isoform in the biology of epithelial–cells [13]. Recent studies have described that ΔNp63
82 overexpressing mice exhibits hyperproliferation, defects in terminal differentiation and an
83 inflamed skin phenotype, demonstrating a key role of ΔNp63 in inflammatory skin disease
84 [17,18].
85
86 We show that, in the normal keratinocytes physiological state, p63 positively regulates
87 iRHOM2, while iRHOM2 antagonizes ΔNp63 expression. In contrast, in hyperproliferative
88 keratinocytes, there is an auto-regulatory feedback loop occurring between ΔNp63 and
89 iRHOM2. We show that p63-iRHOM2 mediated signalling regulates ADAM17 activity and
90 cellular functions including inflammation, proliferation, survival and oxidative defence.
91 Furthermore, we identify SURVIVINas a novel binding partner of iRHOM2 and as a p63
92 target gene. In addition, we also reveal a role of iRHOM2 in the epidermal oxidative defence
93 response via its interaction with Cytoglobin(CYGB), a reported p63 target gene. Our findings
94 implicate a novel signalling pathway involving p63 and iRHOM2 in the control of
95 hyperproliferative skin diseases and squamous oesophageal cancer.

96

97

98 **Results**

99 **p63 regulates iRHOM2 expression in normal keratinocytes**

100 To identify transcriptional regulators of iRHOM2, specifically if the *RHBDF2* gene encoding
101 iRHOM2 may be a direct p63 target, we analyzed the available p63 ChIP-seq dataset
102 performed in human and mouse keratinocytes[19] [20] . This revealed that the human and
103 mouse p63 binding sites are very well conserved at the intragenic region (Fig. 1a and
104 Supplementary Fig. 1a). Furthermore, ChIP-qPCR confirmed that p63 binds to *RHBDF2* gene
105 locus (Fig. 1b). In addition, ChIP-qPCR analysis for the specific binding of p63 was performed
106 with p21 (positive control), Thymidine kinase TK (negative control) and a no-gene region
107 (Chr11) (Supplementary Fig.1b). These data indicate that p63 binds to the intragenic
108 enhancer region of *RHBDF2* and that iRHOM2 is a direct p63 target gene. In addition, we
109 cloned this specific intragenic region, into the pGL3 enhancer plasmid [19], and tested
110 whether the luciferase reporter gene activity is induced by TAp63α and ΔNp63α in HEK293
111 cells (Human Embryonic Kidney cells). As shown in Fig. 1c, both TAp63α and ΔNp63α
112 markedly upregulated luciferase activity. To further investigate whether p63 binding to
113 iRHOM2 intragenic region affects iRHOM2 expression, each p63 isoform (ΔNp63α, ΔNp63β,
114 ΔNp63γ, TAp63α, TAp63β, TAp63γ) was transiently transfected in HEK293 cells. qRT-PCR and
115 western blot analysis showed that overexpression of the p63 isoforms modulate iRHOM2
116 expression, in particular TAp63α and ΔNp63α significantly induce iRHOM2 expression at
117 mRNA and protein levels (Fig. 1d and e). Additionally, depletion of p63 in keratinocytes by a
118 small interfering RNA (siRNA) which targets all p63 isoforms [21] significantly reduced
119 endogenous iRHOM2 protein expression (Fig. 1f) as well as at the mRNA level
120 (Supplementary Fig. 1c). Our data suggest that ΔNp63α, the major p63 isoform expressed in
121 epidermis, is also the major p63 isoform that regulates iRHOM2 in keratinocytes.

122 To further investigate the expression of iRHOM2 in keratinocytes, HaCaT keratinocyte
123 differentiation was induced *in vitro* by adding Ca^{2+} to the culture medium. iRHOM2
124 expression was upregulated upon the induction of differentiation in a time-dependent
125 manner (Supplementary Fig. 1d). ΔNp63, keratin 14 (K14) and involucrin expression was

126 assessed by western blotting to confirm that the keratinocytes were undergoing
127 differentiation. As expected, ΔNp63 and K14, highly expressed under proliferative
128 conditions, were reduced upon the induction of differentiation while involucrin expression
129 was upregulated. Additionally, we also validated by qRT-PCR the increase expression of
130 *RHBDF2* at mRNA levels upon Ca^{2+} shift (Supplementary Fig. 1e) and K14 was used as a
131 control of the differentiation state. Moreover, iRHOM2 is expressed in the cytoplasm and
132 plasma membrane of the basal and suprabasal layers of human epidermis (Supplementary
133 Fig. 1f). Taken together, these results demonstrate that iRHOM2 is a transcriptional target of
134 p63 and suggests that iRHOM2 might be implicated in the regulation of epidermal
135 differentiation.

136 **Distinct regulation of p63 expression in keratinocytes**
137 Examination of the morphology of the stratified epithelia revealed a thicker epidermis in
138 TOC compared with normal interfollicular skin as previously reported [9,22] (Fig. 2a).
139 Immunohistochemistry showed increased p63 expression in the nuclei of the basal and
140 suprabasal layers in TOC epidermis compared to control interfollicular skin (Fig. 2a). To
141 better delineate the basal cells of the epidermis, we also performed immunofluorescence
142 staining for Keratin 14 (K14), a marker of the basal layer (Supplementary Fig. 2a). Similarly,
143 in the immortalised TOC keratinocytes, ΔNp63 was upregulated at the mRNA and protein
144 levels when compared to control keratinocytes (Supplementary Fig. 2b and 2c). Microscopic
145 examination of haematoxylin and eosin-stained skin sections showed no significant
146 difference in the thickness of the *rhbdf2*$^{-/-}$ mice back skin compared to wild-type controls,
147 while the *rhbdf2*$^{-/-}$ mice paw revealed a thinner epidermis compared to *rhbdf2*$^{+/+}$ mice as
148 published previously [12]. Back skin and footpads from *rhbdf2*$^{-/-}$ mice were immunostained for
149 p63 and analysed by confocal microscopy (Fig.2b). *rhbdf2*$^{-/-}$ mice showed increased p63
150 expression in the back skin but had reduced expression in their footpad epidermis
151 compared to *rhbdf2*$^{+/+}$ littermates (Fig. 2b). K14 was also used to delineate the basal cells of
152 the epidermis (Supplementary Fig. 2d), as a "bona fide" target of p63, interestingly, K14
153 follows the same p63 expression pattern. In addition, we also confirmed modulation of p63
154 expression by qRT-PCR and western blot analysis of extracts derived from paw and back skin
155 of *rhbdf2*$^{+/+}$ and *rhbdf2*$^{-/-}$ mice. (Fig. 2c and Supplementary Fig. 2e). To investigate this
156 apparent cell-context regulation of p63 by iRHOM2, we next used short hairpin RNA (shRNA)

157 knockdown of iRHOM2, which was found to increase ΔNp63 protein expression in control
158 keratinocytes, while sh-iRHOM2 TOC keratinocytes resulted in a downregulation of ΔNp63
159 expression (Supplementary Fig. 2f). These observations indicate that, in interfollicular skin,
160 iRHOM2 represses ΔNp63 expression, whilst in hyperproliferative footpad skin and in TOC
161 keratinocytes, iRHOM2 positively regulates ΔNp63 expression.

162 **iRHOM2-ADAM17 axis regulates p63 expression**

163 iRHOM2 regulates the maturation of the multi-substrate ectodomain sheddase enzyme
164 ADAM17 [7,8] and, in TOC derived keratinocytes, there is increased cleavage of ADAM17
165 substrates such as TNFα, IL-6R and EGFR ligands compared to control cells (9). TOC derived
166 keratinocytes exhibit features of a constitutive "wound-healing" phenotype in which the
167 iRHOM2-ADAM17 axis plays a key role in skin barrier maintenance, inflammation and
168 migration [5,9]. Here, the modulation of the iRHOM2-ADAM17 axis on p63 expression was
169 investigated. Western blot analysis (Fig. 3a) revealed that ADAM17 depletion by siRNA led
170 to an increase of ΔNp63 in control keratinocytes, whilst ΔNp63 was downregulated in TOC
171 keratinocytes. These data were consistent with our data above in iRHOM2 knock-down cells
172 (Supplementary Fig. 2f). In agreement, inhibition of ADAM17 using the small molecule TMI-
173 005 increased ΔNp63 in control keratinocytes but decreased its expression in TOC
174 keratinocytes (Fig. 3b). As TOC derived keratinocytes display an inflammatory phenotype [8,9],
175 we next assessed whether the secretion of growth factors and cytokines in these cells may
176 regulate the expression of ΔNp63.

177

178 Surprisingly, we found that conditioned media from TOC derived keratinocytes reduced
179 ΔNp63 expression (Fig. 3c) in control cells. As TNFα is known to induce keratinocyte
180 differentiation and modulate p63 expression [23], keratinocytes treated with PMA (phorbol
181 12-myristate 13-acetate) showed downregulation of ΔNp63 expression in control cells
182 (Supplementary Fig. 3a) confirming previous studies [24,25]. However, the addition of
183 conditioned media from TOC keratinocytes to TOC keratinocytes with shRNA mediated
184 knockdown of iRHOM2 showed a restoration of ΔNp63 expression (Fig. 3d). These data
185 suggested that "the environment" of cell surface shed cytokines and growth factors can
186 regulate ΔNp63 expression in a cell context dependent manner.

187

188 To examine this putative p63-iRHOM2-ADAM17 axis further, western blot analysis of both
189 control and TOC keratinocytes with p63 siRNA knockdown (Fig. 3e) revealed reduced
190 expression of both iRHOM2 and ADAM17. As TOC keratinocytes are characterised by
191 increased ADAM17 maturation and shedding of its substrates [9], we assessed the role of p63
192 in the regulation of ADAM17 protease activity. We demonstrated that depletion of p63 in
193 both control and TOC keratinocytes resulted in decreased ADAM17 maturation and
194 consequently, a reduction in the "shedding" of TGFα, TNFα and IL-6R (Fig. 3f). To investigate
195 the mechanism by which p63 regulates ADAM17 expression and its downstream pathway,
196 we analyzed the available p63 ChIP-seq dataset performed in human and mouse
197 keratinocytes[19,20]. This revealed that the human and mouse p63 binding sites are very well
198 conserved at the intragenic region (Fig. 3g and Supplementary Fig. 3b). Furthermore, ChIP-
199 qPCR confirmed that p63 binds to the *ADAM17* gene locus (Fig. 3h). These data indicate that
200 *ADAM17* is a direct p63 target gene. To further investigate whether p63 binding to *ADAM17*
201 intragenic region affects ADAM17 expression, p63 isoforms were transiently transfected in
202 HEK293 cells. In addition, qRT-PCR and western blot analysis showed that overexpression of
203 TAp63α and ΔNp63α significantly induce ADAM17 at both mRNA and protein level
204 (Supplementary Fig. 3c and 3d). Similarly, *ADAM17* is also known to be a p73 target gene,
205 another p53 homologue [26], such as p63. Thus, these results revealed that p63 can directly
206 regulate both iRHOM2 and ADAM17 expression.

207 Additionally, in our previous study [12], we have shown that downregulation of iRHOM2 in
208 both control and TOC keratinocytes was associated with reduced cell proliferation and
209 migration. Here we found that depletion of p63 also reduced both proliferation and
210 migration in control and TOC cell lines (Supplementary Fig. 3e and 3f).

211

212 **iRHOM2-p63 axis modulates resistance to apoptosis**

213 TOC epidermis displays improved barrier function, hyperproliferation and thickening of the
214 palmoplantar [9,12]. As exposure to ultraviolet B (UV-B) light is an environmental stressor for
215 basal keratinocytes, we investigated the cellular response in TOC keratinocytes. Upon UV-B
216 treatment, TOC keratinocytes showed greater resistance to cell death compared to control
217 keratinocytes as assessed by annexin-V staining using flow cytometry (Fig. 4a). Furthermore,
218 control and TOC keratinocytes depleted for iRHOM2 exhibited an induction of apoptosis

219 (Supplementary Fig. 4a). Depletion of iRHOM2 in TOC keratinocytes increased sensitivity to
220 UV-B induced apoptosis (Fig. 4b). Moreover, both cell lines depleted for p63 demonstrated
221 induction of apoptosis following UV-B treatment (Supplementary Fig. 4b). These data
222 suggest that iRHOM2 and p63 are involved in the regulation of the keratinocyte apoptotic
223 pathway. Understanding the mechanism(s) through which TOC keratinocytes displayed
224 resistance to cell death, the expression of inhibitors of apoptosis proteins (IAP) was
225 investigated. Western blot analysis revealed an increased expression of SURVIVINin TOC
226 keratinocytes compared to control cells whilst expression of the other members of the IAP
227 family were unchanged (Supplementary Fig. 4c). We also investigated the effect of UV-B
228 stimulation on iRHOM2, ΔNp63 and SURVIVNexpression by western blot analysis. We first
229 confirmed that the cells undergo apoptosis by assessing the expression of PARP, and
230 observed lower levels of PARP cleavage in TOC keratinocytes after UV-B exposure in
231 comparison to control cells. iRHOM2, ΔNp63 and SURVIVIN expression was virtually absent
232 in UV-B exposed control keratinocytes but only slightly lower in TOC keratinocytes (Fig. 4c).
233
234 To explore this putative regulation of SURVIVINby iRHOM2 further, confocal analysis
235 revealed an increase in SURVIVINexpression in the cytoplasm and the nuclei of basal layer of
236 keratinocytes in TOC epidermis, compared to control interfollicular skin (Fig. 4d).
237 Immunostaining in *rhbdf2*$^{-/-}$ mouse skin showed increased levels of SURVIVINexpression in
238 the back skin but reduced levels in their footpads in comparison to *rhbdf2*$^{+/+}$ littermate
239 controls (Fig. 4e). In addition, we also confirmed the modulation of SURVIVINexpression by
240 western blot analysis of protein extracts taken from back skin and paw of *rhbdf2*$^{+/+}$ and
241 *rhbdf2*$^{-/-}$ mice (Supplementary Fig. 4d).

242 In agreement with data obtained from *rhbdf2*$^{-/-}$ mice, depletion of iRHOM2 resulted in an
243 increase of SURVIVINprotein expression in control keratinocytes and a reduction in TOC
244 keratinocytes (Supplementary Fig. 4e). To further explore the molecular mechanism by
245 which iRHOM2 regulatesSURVIVIN, we investigated whether the two proteins are associated
246 in a complex. Co-immunoprecipitation analysis showed that endogenous iRHOM2 was able
247 to efficiently immunoprecipitate SURVIVINin control keratinocytes (Fig. 4f) and that
248 endogenous SURVIVINforms a complex with iRHOM2 (Supplementary Fig. 4f). Taken
249 together our data demonstrated that iRHOM2 is involved in the regulation ofSURVIVIN.

250

251 As the depletion of p63 and iRHOM2 in both control and TOC keratinocytes induced
252 apoptosis, we explored a possible regulation of SURVIVINby p63. Prior studies have shown
253 that SURVIVINis negatively regulated by wild -type p53 but not mutated p53 [27]. To identify
254 transcriptional regulators of *BIRC5*, we analysed the available p63 ChIP-seq dataset
255 performed in human and mouse keratinocytes[19,20]. This revealed that the human and mouse
256 p63 binding sites are very well conserved at the intergenic region. (Fig. 4g and
257 Supplementary Fig. 4g). ChIP-qPCR revealed that p63 binds to *BIRC5* gene locus (Fig. 4h).
258 These data indicate that *BIRC5* is a direct p63 target gene. To further investigate whether
259 p63 binding to *BIRC5* intergenic region affects SURVIVINexpression, p63 isoforms were
260 transiently transfected in HEK293 cells. Results showed by qRT-PCR analysis that cells
261 overexpressing TAp63α and ΔNp63α induce significantly *BIRC5* at mRNA level
262 (Supplementary Fig. 4h). Western blotting analysis confirmed the same results
263 (Supplementary Fig. 4i). In addition, depletion of p63 by siRNA reduced endogenous
264 expression of SURVIVINin both control and TOC keratinocytes (Supplementary Fig. 4j). These
265 findings support a model of reciprocal regulation between iRHOM2 and ΔNp63 in
266 hyperproliferative keratinocytes that may play a role in the resistance to apoptosis via
267 modulation of SURVIVIN.

268 **iRHOM2-p63 axis regulates oxidative stress**

269 Previous studies have shown that oxidative stress contributes to a form of palmoplantar
270 keratoderma (pachyonychia congenita) [28], as well as inflammation [29], and may suppress
271 apoptosis and promote proliferation [30]. Therefore, we investigated whether the iRHOM2
272 pathway could play a role in ROS (reactive oxygen species) regulation. We examined the
273 production of ROS in the cells using DHE (Dihydroethidium) dye by flow cytometry. In this
274 assay ROS convert non-fluorescent DHE to fluorescent ethidium, which then intercalates
275 into DNA. We found that TOC keratinocytes showed increased level of ROS compared to
276 control cells (Fig. 5a). However, a reduction in DHE stained cells was observed in both
277 control and TOC keratinocytes depleted for iRHOM2 (Fig. 5b). We also showed a significant
278 decrease of ROS level in control and TOC keratinocytes depleted for iRHOM2 by flow
279 cytometry (Supplementary Fig. 5a). Similarly, we also assessed the role of p63 in the
280 regulation of ROS. An increase of ROS production in control keratinocytes depleted for p63

281 was observed while the levels were downregulated in TOC cells silenced for p63
282 (Supplementary Fig. 5b).
283
284 In order to explore a potential mechanism through which the p63-iRHOM2 axis may control
285 oxidative stress in TOC keratinocytes, we evaluated the expression of genes associated with
286 antioxidant pathways such as *NQO1* (NAD-(P)H:quinone oxidoreductases), *HMOX1* (Heme
287 Oxygenase 1), *SOD1* (Superoxide Dismutase 1) and *CYGB* Cytoglobin) by qRT-PCR. We
288 observed a down regulation of these antioxidant genes in TOC keratinocytes compared to
289 control (Fig. 5c) which are correlated with the increase levels of ROS in TOC keratinocytes.
290 Interestingly, dysregulation of NRF2 was reported to contribute to palmoplantar
291 keratoderma [28] . We investigate whether NRF2 may play a role in our pathway. Our data
292 showed that *NRF2* is not modulated at mRNA levels in control and TOC keratinocytes
293 (Supplementary Fig. 5c) as well in the cells depleted for iRHOM2 (Supplementary Fig. 5d).
294 Our studies then focussed on *CYGB* as it is a known p63 target gene [31] and ROS scavenger [32-
295 34] plus *CYGB* is also transcriptionally down-regulated in TOC oesophagus [35,36]. Confocal
296 analysis showed reduced CYGBexpression in the basal layer of TOC epidermis compared to
297 control interfollicular skin (Supplementary Fig. 5e). We also confirmed that p63 depletion
298 led to a reduction of *CYGB* in control cells by qRT-PCR. However, in TOC cells, p63 siRNA
299 resulted in an upregulation of *CYGB* expression (Supplementary Fig. 5f). These findings
300 observed in TOC cells with p63 siRNA are correlated with the modulation of ROS observed in
301 those cells.
302
303 To further support a role for iRHOM2 in CYGBregulation, an increase in Cygb expression was
304 observed by confocal analysis in both back skin and footpad from *rhbdf2*$^{-/-}$ mice compared
305 to *rhbdf2*$^{+/+}$ (Fig. 5d). In addition, we also confirmed modulation of CYGB expression by
306 western blot analysis of protein extracts derived from the back skin and paw of *rhbdf*2$^{+/+}$
307 and *rhbdf*2$^{-/-}$ mice (Fig. 5e). Similarly, shRNA knock-down of iRHOM2 showed an
308 upregulation of CYGBin both control and TOC keratinocytes by western blot analysis (Fig.
309 5f). These data are correlated with the observed reduction of ROS production in iRHOM2-
310 depleted cells and suggest a possible interaction may be occurring between iRHOM2
311 andCYGB. To investigate this possible interaction, Proximity-ligation assay (PLA) was
312 performed in control keratinocytes and showed intense signals corresponding to formation

313 of complexes between iRHOM2 and CYGB(Fig. 5g). Also, co-immunoprecipitation analysis
314 showed that endogenous CYGBwas able to efficiently immunoprecipitate iRHOM2 in control
315 keratinocytes (Supplementary Fig.5g). These data indicate that iRHOM2 interacts with and
316 repressesCYGB, plus suggest both p63 and iRHOM2 participate in regulating the oxidative
317 stress response.

318

319 **SFN suppresses p63- iRHOM2 pathway in TOC**

320 Oxidative stress has been linked previously to palmoplantar keratoderma associated with
321 Keratin 16 (K16) mutations, and the use of SFN (Sulforaphane), a natural isothiocyanate
322 compound found in cruciferous vegetables, rescued the palmoplantar keratoderma
323 phenotype in K16$^{-/-}$ mice [28]. Furthermore our recent study [12] has shown that *rhbdf2*$^{-/-}$ mice
324 footpad showed a thinner epidermis, demonstrating that iRHOM2 regulates
325 hyperproliferation and thickening of the palmoplantar epidermis. To explore whether SFN
326 could affect TOC keratinocytes, cells were treated with this compound and analysed for ROS
327 production by flow cytometry. Data showed that SFN treatment significantly reduced ROS
328 production in TOC keratinocytes (Fig. 6a). Moreover, the treated TOC cells showed a
329 significant reduction in cell proliferation (Fig. 6b) and were undergoing apoptosis (Fig. 6c).
330 To investigate if SFN could regulate p63-iRHOM2 and associated downstream pathways,
331 western blot analysis was performed and showed a downregulation of iRHOM2, ΔNp63 and
332 SURVIVINbut an upregulation of CYGBfollowing SFN treatment (Fig. 6d). In agreement with
333 our previous report demonstrating that iRHOM2 regulates the stress-response keratin, K16
334 [12], a downregulation of K16 expression (Fig. 6d) and the collapse of K16 filaments network
335 upon SFN treatment in TOC keratinocytes was observed (Fig. 6e). It has been reported that
336 apoptosis can result in keratin solubilisation, filament organization and collapse [37]. In
337 support of the positive feedback loop occurring between ΔNp63 and iRHOM2 in
338 hyperproliferative keratinocytes, TOC keratinocytes silenced for p63 also demonstrated a
339 downregulation of K16 (Supplementary Fig. 5h). Together, these data support the
340 hypothesis that SFN inhibits the p63-iRHOM2 signalling pathway. SFN treatment reduced
341 TOC-cell proliferation similarly to p63 (Supplementary Fig. 3e) or iRHOM2 [12]
342 downregulation. These cells also showed a reduction of ADAM17 mediated shedding of
343 TGFα and IL-6R (Fig. 6f). Importantly, SFN treatment restored CYGBexpression and reduced

344 ROS levels. Moreover, SFN-treated cells also displayed a reduced SURVIVINexpression and
345 were more sensitive to cell death. The increase in apoptosis was confirmed with the
346 activation of p53 by phosphorylation of serine 15 (Fig. 6d).These findings indicated that SFN
347 reduces the activation of p63-iRHOM2 pathway in TOC keratinocytes, resulting in reduced
348 oxidative stress, inflammation, proliferation, stress-response K16 and increased apoptosis.
349
350 **Discussion**
351
352 Gain-of-function mutations in *RHBDF2*, the gene encoding iRHOM2, underlie Tylosis with
353 Oesophageal Cancer (TOC)[5], a syndrome characterized by palmoplantar thickening. We have
354 recently shown the role of iRHOM2 in determining footpad thickness in humans and mice [12],
355 with *rhbdf2*$^{-/-}$ mice displaying a thinner footpad epidermis, the opposite of the phenotype
356 observed in human TOC palmoplantar epidermis. These data support an important role for
357 iRHOM2 in regulating the epithelial response to stress. In this present study we provide new
358 insights into the functional role of iRHOM2 in skin epidermal homeostasis. Here, iRHOM2
359 has been identified as a new transcriptional target of p63 that is regulated in a cell context
360 dependent manner. Considering that iRHOM2 is a key regulator of EGFR signalling and that
361 iRHOM2 mutations cause an increase in the maturation and activity of ADAM17, we
362 investigated its downstream pathway. Our data revealed that p63 has an impact on
363 ADAM17 and its associated substrates demonstrating a role of p63 in inflammatory skin
364 diseases. In addition, we are also reporting that iRHOM2-ADAM17 axis regulates p63
365 expression. These findings highlight a novel regulation linking iRHOM2 and p63 and suggest
366 that some common pathways are occurring in keratinocyte homeostasis. We have recently
367 validated a model of study [12] in which we have established that mouse footpad skin and
368 human TOC keratinocytes are considered to be a hyperproliferative model, compared to
369 murine back skin and normal keratinocytes, which are equivalent to physiological
370 conditions.
371
372 In the normal physiological state, such as in control keratinocytes or in mouse back skin, p63
373 positively regulates iRHOM2 while it antagonises ΔNp63 expression (Fig. 7). Thus, in this
374 context, p63 depletion leads to a down regulation of its novel or known target genes such as
375 iRHOM2, ADAM17, SURVIVIN and CYGB[31]. In contrast, iRHOM2 downregulation "de-
376 represses" p63 which in turn activates its downstream target genes such as

377 SURVIVINandCYGB. Our findings emphasise a critical role for the p63-iRHOM2 axis in normal
378 skin. These data support previous findings showing significant roles for both p63 [26,27,31] and
379 iRHOM2 [12] in regulating cellular proliferation, migration and inflammation.
380
381 In the hyperproliferative state, TOC keratinocytes depleted for iRHOM2 and *rhbdf2*$^{-/-}$
382 footpad skin showed a downregulation of ΔNp63 expression. Our data highlight the fact that
383 inflammation in TOC keratinocytes supports a hyperproliferative phenotype with ΔNp63
384 overexpression. These findings indicate that iRHOM2 positively regulates ΔNp63 expression
385 in TOC. Consequently, we observed an increased expression of p63 target genes in
386 hyperproliferative keratinocytes. Moreover, p63 depletion reduces iRHOM2 expression in
387 TOC keratinocytes. Thus, this indicates that there is an auto-regulatory feedback loop
388 occurring between iRHOM2 and ΔNp63 in the hyperproliferative state (Fig. 7), with similar
389 regulation in proliferation, migration and inflammation.
390
391 Towards understanding the mechanisms through which TOC keratinocytes responded to
392 stressors, we investigated how these cells respond to UVB treatment. This study allow us to
393 identify survivin as a p63 target gene, which contributes to apoptosis resistance [38],
394 confirming previous reports attributing a role of ΔNp63 in cell survival [39,40]. In addition, we
395 have shown a key role for iRHOM2 in apoptosis via its direct regulation of SURVIVIN. Thus,
396 in TOC keratinocytes, p63 siRNA or shRNA knock-down of iRHOM2 induces apoptosis and
397 shows SURVIVINdown regulation. These observations confirmed previous studies
398 demonstrating that SURVIVINis often upregulated in cancer and dysplasia driving resistance
399 to cell death and contributing to progression of neoplasia [41].
400
401 Hyperproliferation and dysregulation of apoptosis are related to ROS production as it plays a
402 role in these processes [30]. We have identified *CYGB*, a known p63 target gene [31], as a key
403 modulator of ROS production in TOC keratinocytes. Prior studies have associated CYGBwith
404 cancer suppression [42] especially in oesophageal cells [36], and reported a transcriptional
405 downregulation of *CYGB* in TOC . We confirmed low levels of CYGBexpression in TOC and
406 now identify CYGBas a novel interacting binding partner of iRHOM2**.** Thus, either the
407 depletion of p63 or iRHOM2 in TOC keratinocytes, as well in *rhbdf2*$^{-/-}$ footpad skin, increases

408 CYGBexpression, which in turn dampens ROS release, indicating that the iRHOM2-p63
409 pathway influences maintenance of the redox status.
410
411 In TOC keratinocytes, the natural antioxidant compound, sulforaphane (SFN) reduced ROS
412 production and strikingly inhibited the iRHOM2-p63 pathway which can drive survival and
413 inflammation. Previous studies have reported that SFN possesses potent chemopreventive
414 efficacy in cancers [43] by inducing apoptosis [44], NRF2 mediated induction of phase II
415 detoxifying enzymes [45], protecting multiple organs from oxidative injuries [46] and reducing
416 the inflammatory response [47]. Additionally, it has been well established that these different
417 mechanisms act synergistically [48]. Consistent with a recent study, oxidative stress and
418 dysfunctional NRF2 underlies the palmoplantar keratoderma disorder pachyonychia
419 congenita with SFN treatment reducing the aberrant keratinisation in *K16* $^{-/-}$ mice [28]. Our
420 findings demonstrate that SFN could also be used pharmacologically in TOC keratinocytes to
421 target the downstream effects of the iRHOM2-p63 pathway, especially through
422 CYGBinduction. Thus, it is noteworthy to observe that SFN seems to mimic the depletion of
423 p63 or iRHOM2 in TOC keratinocytes. As we have shown previously that *rhbdf2*$^{-/-}$ mice
424 footpad showed a thinner epidermis [12] with absence of K16 expression, SFN treatment may
425 have a similar impact on the hyperproliferative skin and oesophageal phenotype in TOC [28].
426 This study supports the model of the iRHOM2-p63 pathway regulating inflammation,
427 hyperproliferation, oxidative stress and cell survival. Thus targeting of the iRHOM2-p63 axis
428 in keratinisation disorders and dysplasia could have therapeutic potential.
429
430 **Figure Legends**
431 **Figure 1**: **Identification of iRHOM2 as a p63 target gene in keratinocytes.**
432 **(a)** Screenshot of the UCSC genome browser from ChIP-seq analysis of normal human
433 primary keratinocytes with two different antibodies (4A4, pan-p63 and H129, α-specific).
434 The ChIP-seq study was previously reported. **(b)** Chromatin immunoprecipitation in control
435 keratinocytes (CTRL) with anti-pan p63 (H137) and anti-IgG antibodies followed by
436 quantitative PCR (ChIP-qPCR) analysis showed that p63 binds to *RHBDF2* intragenic region.
437 Error bars represent SEM of three independent experiments and Student's two-tailed *t*-test
438 value is shown; $p < 0.001$ (***). **(c)** Luciferase assay for *RHBDF2* gene locus. The construct

439 was transiently transfected into HEK293 cells in the absence (-) or in the presence of
440 ΔNp63α or TAp63α. The (+) control corresponds to IRF6p229-Luc plasmid. The activity of the
441 intragenic region was measured by luciferase assay and values are expressed relative to (-)
442 set to 1. Data were analysed using two-tailed Student's *t*-test ($p < 0.05$ (*), $p < 0.01$ (**) and
443 $p < 0.001$ (***)). **(d)** qRT-PCR for *RHBDF2* in HEK293 cells transfected with TA and ΔNp63
444 isoforms. The graph represents means and SEM of three biological replicates after 9 hours
445 of transfection. Statistical analysis was performed by Student's two-tailed *t*-test comparing
446 pcDNA transfected cells to other samples. **(e)** Immunoblotting of HEK293 cells over-
447 expressing p63 isoforms, showed TA and ΔNp63 isoforms (α-pan p63) and iRHOM2
448 expression after 9 hours of transfection. GAPDH was used as loading control. The graph
449 represents the means of the quantification, using ImageJ software, from three independent
450 experiments relative to GAPDH. Error bars represent SEM and Student's two-tailed *t*-test
451 values are given $p < 0.05$ (*). **(f)** Representative Western blotting (WB) shows expression of
452 ΔNp63 and iRHOM2 in normal keratinocytes (CTRL) treated with non-targeted protein (NTP)
453 or p63 siRNAs. GAPDH was used as a loading control.

454

455 **Figure 2**. **Distinct regulation of p63 in normal and hyperproliferative keratinocytes.**

456 **(a)** Representative images of H&E stained sections, displaying a hyperproliferative epidermis
457 in TOC compared to normal interfollicular skin. Confocal microscopy analysis shows p63 (α-
458 pan p63) expression in TOC and in control interfollicular skin. DAPI (blue) is used as a nuclear
459 stain. Scale bars: 20 µm. Graph represents quantifications of p63 expression in ratio with the
460 nuclei from three human samples. Student's two-tailed *t*-test value is shown, $p < 0.01$ (**).
461 **(b)** Representative H&E stained back skin and fore-paw sections from 20-week-old *rhbdf2*$^{+/+}$
462 and *rhbdf2*$^{-/-}$ mice. Scale bar: 20 µm. Confocal analysis of p63 (α-pan p63) expression was
463 performed in back skin and fore-paw sections of *rhbdf2*$^{+/+}$ and *rhbdf2*$^{-/-}$ mice. Scale bar: 20
464 µm. (**c)** qRT-PCR for *ΔNp63* from mRNA extracted from back skin and fore-paws of *rhbdf2*$^{+/+}$
465 and *rhbdf2*$^{-/-}$ mice. The graph shows n=6 of each genotype. The statistical analysis was
466 performed using Student's two-tailed *t*-test ($p < 0.05$ (*), $p < 0.01$ (**)).

467

468 **Figure 3. iRHOM2-ADAM17 axis regulates p63 expression.**

469 **(a)** Expression of ADAM17 and ΔNp63 by WB in control (CTRL) and TOC keratinocytes
470 transfected with non-targeting pool (NTP) and ADAM17 siRNA. **(b)** Immunoblotting of
471 ΔNp63 expression performed in CTRL and TOC keratinocytes treated with and without TMI-
472 005 for 24 h. **(c)** Immunoblotting for ΔNp63 in CTRL keratinocytes and **(d)** in Sh Scr
473 (Scramble) and Sh iRHOM2 TOC keratinocytes treated with or without conditioned media
474 (CM) for 24 h. GAPDH was used as a loading control. **(e)** WB analysis for ΔNp63, iRHOM2
475 and ADAM17 in normal and TOC keratinocytes with NTP and p63 siRNA. TUBULIN was used
476 as a loading control. All the quantifications included were performed by ImageJ software in
477 comparison to the loading control in three independent experiments. Student's t test was
478 used, ($p<0.05$ (*) and $p<0.01$ (**)). **(f)** Levels of TNF-α, TGF-α and IL-6R were assessed by
479 ELISA from the supernatant of NTP, p63 and ADAM17 siRNAs in CTRL and TOC keratinocytes.
480 Data are expressed as mean with SEM from four experiments. Statistical analysis was
481 compared to NTP siRNA CTRL or TOC using one way ANOVA Dunnett's multiple comparison
482 test ($p<0.05$ (*), $p<0.01$ (**) and $p<0.001$(***)). **(g)** Screenshot of the UCSC genome browser
483 from ChIP-seq analysis of normal human primary keratinocytes with two different
484 antibodies (4A4, pan-p63 and H129, α-specific). The ChIP-seq study was previously reported.
485 **(h)** Chromatin immunoprecipitation in control keratinocytes (CTRL) with anti-pan p63 (H137)
486 and anti-IgG antibodies followed by quantitative PCR (ChIP-qPCR) analysis showed that p63
487 binds to *ADAM17* intragenic region. Error bars represent SEM of three independent
488 experiments. For statistical evaluation Student's two tailed t-test was used ($p < 0.01$ (**)).

489

490 **Figure 4. iRHOM2-p63 axis regulates apoptosis in keratinocytes by modulating SURVIVIN.**

491 **(a)** Percentage of apoptotic cells was quantified by using flow cytometric analysis of
492 annexin-V-positive populations in control (CTRL) and TOC keratinocytes after 24 h of UV-B
493 irradiation (10 or 25 mJ cm^{-2}). Data represent means and SEM of four experiments.
494 Statistical analysis was performed comparing TOC keratinocytes treated with 10 or 25
495 mJ/cm^2 and CTRL cells treated at the same doses using Student's two-tailed *t*-test ($p <$
496 0.05(*)). **(b)** Percentage of apoptotic cells was quantified by using flow cytometric analysis
497 of annexin-V-positive populations in Sh Scr and Sh iRHOM2-transfected TOC keratinocytes
498 irradiated with 10 or 25 mJ/cm^2 for 24 h. Data represent mean with SEM of five
499 independent experiments. For statistical evaluation Student's two tailed *t*-test was used

500 (p<0.05 (*), p < 0.01 (**)). **(c)** Immunoblotting for PARP, cleaved PARP (PARPc), ΔNp63,
501 iRHOM2 and SURVIVIN in UVB irradiated CTRL and TOC keratinocytes with 10 or 25 mJ cm^{-2}
502 UV-B treatment. GAPDH is used as a loading control. **(d)** Representative confocal microscopy
503 images from immunostaining of SURVIVIN in normal and TOC skin. DAPI (blue) is used as a
504 nuclear stain. Scale bar: 20 µm. **(e)** Immunostaining of SURVIVIN was performed in back skin
505 and fore-paw sections of *rhbdf2*$^{+/+}$ and *rhbdf2*$^{-/-}$ mice by confocal microscopy. DAPI (blue) is
506 used as a nuclear stain. Scale bar: 20 µm. **(f)** CTRL keratinocyte lysates were
507 immunoprecipitated using an anti-iRHOM2 antibody and immunoblotted with anti-
508 SURVIVIN antibody. **(g)** Screenshot of the UCSC genome browser from ChIP-seq analysis of
509 normal human primary keratinocytes with two different antibodies (4A4, pan-p63 and H129,
510 α-specific). The ChIP-seq study was previously reported. **(h)** Chromatin immunoprecipitation
511 in control keratinocytes (CTRL) with anti-pan p63 (H137) and anti-IgG antibodies followed by
512 ChIP-qPCR analysis showed that p63 binds to the *BIRC5* intergenic region. Error bars
513 represent SEM of three independent experiments. For statistical evaluation Student's two
514 tailed *t*-test was used (p < 0.01 (**)).

515

516 **Figure 5. iRHOM2 regulates oxidative stress in hyperproliferative keratinocytes.**

517 **(a**) Quantification of Dihydroethidium (DHE) staining in control (CTRL) and TOC
518 keratinocytes by flow cytometry. Data are expressed as mean and SEM of three
519 independent experiments. Statistical analysis was performed to compare CTRL and TOC cells
520 using Student's two-tailed *t*-test (p < 0.01(**)). **(b)** DHE staining (red) in live Sh Scr or Sh
521 iRHOM2-transfected CTRL and TOC keratinocytes by confocal microscopy. Hoechst 33342
522 (blue) was used to identify nuclei. **(c)** qRT-PCR of *HMOX1*, *NQO1*, *SOD* and *CYGB* in TOC
523 keratinocytes was assessed as fold change compared to CTRL cell expression (dashed line).
524 The graph represents means and SEM of three biological replicates. Statistical analysis was
525 performed comparing CTRL and TOC keratinocytes using Student's two-tailed *t*-test (p <
526 0.05(*), p < 0.01(**), p < 0.001(***)). **(d)** Immunostaining of CYGB was performed in fore-
527 paw and back skin sections of *rhbdf2*$^{+/+}$ and *rhbdf2*$^{-/-}$ mice by confocal microscopy. DAPI
528 (blue) is used as nuclear stain. Scale bar: 20 µm. **(e)** Representative WB for CYGB expression
529 from proteins extracted from back skin and fore-paw of *rhbdf2*$^{+/+}$ and *rhbdf2*$^{-/-}$ mice. GAPDH
530 was used as a loading control. **(f)** WB analysis of CYGB in Sh Scr and Sh iRHOM2-transfected

531 CTRL and TOC keratinocytes. GAPDH was used as a loading control. **(g)** Representative
532 confocal images from PLA experiments between iRHOM2 and CYGB in control keratinocytes.
533 PLA between K6 and K16 was performed as a positive (+) control, while no primary
534 antibodies were applied in negative (-) control.

535

536

537 **Figure 6. SFN represses iRHOM2-p63 pathway in TOC**

538 **(a)** Quantification of DHE staining by flow cytometry in TOC keratinocytes treated with
539 dimethyl sulfoxide (DMSO; the vehicle control), and sulforaphane (SFN) (10 µM) for 24 h. **(b)**
540 Growth curves of TOC cells cultured with SFN (10 µM) or DMSO for 0, 24 and 48 hrs post
541 treatment. Data are expressed as mean $\pm$ SEM. **(c)** Percentage of apoptotic cells was
542 quantified by using flow cytometry analysis of annexin-V- positive populations detected
543 after 24 h incubation with SFN (10 µM) or DMSO, in TOC cells. Bars represent mean values
544 with SEM of four experiments. **(d)** Immunoblotting of lysates from TOC keratinocytes
545 treated with SFN (10 µM) or DMSO for 24 h and analysed for ΔNp63, iRHOM2, SURVIVIN,
546 K16, p53, phopho-p53 and CYGB expression. GAPDH is used as a loading control. **(e)**
547 Immunofluorescence staining of K16 in TOC cells after 0, 6 and 24 hours of SFN incubation.
548 Scale bar: 20 µm. **(f)** ELISA for TGF-α and IL-6R with the supernatants of TOC cells treated
549 with SFN (10 µM) or DMSO for 24 h. All data are expressed as mean and SEM of three
550 experiments. Statistical analysis was performed by Student's two-tailed *t*-test ($p<0.05$ (*)
551 and $p<0.01$ (**)).

552

553 **Figure 7. Proposed model.**

554 Model illustrating the regulation of iRHOM2-p63 pathway under normal and
555 hyperproliferative states.

556 **Materials and Methods**

557 **Cell Culture and reagents**

558 TOC cells are immortalized keratinocytes from a Tylosis patient carrying the UK *RHBDF2*
559 mutation have been describedpreviously [5].. Control keratinocytes carrying the same
560 immortalization with human papilloma virus (HPV-16) open reading frames E6 and E7 as TOC
561 cells. Cells were cultured in DMEM (Sigma), supplemented with 10% foetal bovine serum
562 (FBS), 1% penicillin–streptomycin (pen-strep), 100uM L-Glutamine (Sigma) and keratinocyte
563 growth supplement RM+ (RM+: containing EGF). HaCaT and HEK293 cells were cultured in
564 DMEM supplemented with 10% FBS, 1% pen-strep and 100uM L-Glutamine. All cells were
565 cultured in sterilized conditions at 37°C with 5% of CO_2. *RHBDF2* or negative scrambled shRNA
566 for control and TOC keratinocytes were previously described [12].
567 Antibodies
568 The list of the used antibodies are reported in Supplementary Information (Supplementary
569 Table 1) .

570 **Treatments**

571 For treatment (UV-B, Phorbol 12-myristate 13-acetate (PMA), condition media (CM),
572 TMI005, Ca^{2+} and Sulforaphane (SFN)), cultured cells were plated at the density of $2x10^5$
573 cells in 6-well plates and allowed to attach overnight at 37˚C, after 24 h, cells were treated.
574 For UV-B, cells were irradiated at 10 and 25 mJ/cm^2. After UVB irradiation, the media was
575 aspired and fresh culture medium was added (samples untreated were just changed with
576 fresh medium). The cells were then harvested at 24 h post irradiation. For PMA (Sigma)
577 treatment, the media was supplemented by the addition of 250 ng/ml PMA for 24 h. In
578 condition media experiments, media from TOC keratinocytes, was centrifuged to eliminate
579 any cells, then filtered using 0.2 µm filter (Millipore) and diluted in complete media (1:2).
580 After these procedures the media was added to the cells for 24 h. For TMI005 (Apratastat,
581 1507 Axon Medchem UK) was dissolved in dimethyl sulfoxide (DMSO) and stock solution
582 was freshly prepared and added to the cells at the final concentration of 500 nM for 24 h.
583 The same DMSO concentration used to dilute the TMI005 was utilised as a negative control.
584 To induce differentiation, calcium (2mM) was added in the medium with 2% of FBS, when
585 the cells until reaching approximately 90% confluence to induced differentiation. SFN was
586 purchased from Sigma and was dissolved in dimethyl sulfoxide (DMSO) at the concentration
587 of 40 mg/ml for the stock solution. SFN was added to cell cultures to obtain the final
588 concentration of 10 µM, samples were analysed after 24 and 48 hours post treatment.

589 **ChIP assay**

590 . Chromatin was prepared from normal keratinocytes and immunoprecipitated with
591 antipan-p63 (H137) overnight at 4°C. ChIP assays were performed as previously described[21].
592 DNA extraction was carried out with phenol–chloroform. Purified DNA was diluted in water
593 and subjected to qRT-PCR. Primer sequences used: ADAM17 F: 5'-
594 CCTCACAATACTCAGCAAAA -3', ADAM17 R: 5'- AGTCAGTAGGAGTGATTATG-3'; RHBDF2 F: 5'-
595 TGTGCCCTTGCTTACCCCTG -3', RHBDF2 R: 5'- CACTCATTTGCTCCTCCAGAC-3'; BIRC5 F: 5'-
596 CTCCTTTCCTGGTGCACCT-3', BIRC5 R: 5'- CGGGGTGTGGTCCCTTTGGA-3'; TK F: 5'-
597 GTGAACTTCCCGAGGCGCAA-3', TK R: 5'-GCCCCTTTAAACTTGGTGGGC-3'; p21 F: 5'-
598 ATGTATAGGAGCGAAGGTGCA-3', p21 R: 5'-CCTCCTTTCTGTGCCTGAAACA-3'; Chr11 F: 5'-
599 TTGCATATAAAGGAAACTGAAATGCT-3', Chr11 R: 5'-TTACTGCCATGGGTCCGTATC-3'.

600 **Transfection**

601 HEK293 cells were transfected by using Lipofectamine 2000 reagent (Invitrogen) at a 1:2
602 (ml/mg) ratio with DNA, using 5 mg of plasmid DNA. The plasmids for p63 overexpression
603 were a generous gift from Dr Eleonora Candi.

604 **Gateway Cloning and Luciferase Reporter Assays**

605 To generate an *RHBDF2* promoter reporter vector, recombinant plasmids were constructed
606 using the Gateway cloning system (Invitrogen). A genomic fragment corresponding to the
607 promoter region of *RHBDF2* was PCR amplified using primers flanked by directional *attB*
608 sites, after which this fragment was integrated into the pDONR221 gateway donor vector
609 (Invitrogen) using BP clonase (Invitrogen). The following, *attB*-flanked, primers were used
610 for the amplification of the *RHBDF2* promoter region –
611 Forward:GGGGACAAGTTTGTACAAAAAAGCAGGCTACCTGGAGGCTCACTCCAC
612 TCT Reverse: GGGGACCACTTTGTACAAGAAAGCTGGGTTGGGATTACAGGCATGAG.

613 After transformation of OneShot TOP10 chemically competent *E.coli* (Thermo Fisher) and
614 selection using kanamycin-containing LB medium, this vector was purified and analysed by
615 restriction digestion using NaeI and HpaI restriction endonucleases. Entry clones with
616 correct integration were then used to clone the promoter sequence into a modified pGL3-
617 Enhancer vector (modified to contain *attR* integration sites) using LR clonase (invitrogen).
618 Once again, these vectors were used to transform OneShot TOP10 competent *E.coli*, which
619 were selected using LB medium containing ampicillin, purified, and analysed for correct
620 integration by restriction digestion using EcoNI and NheI endonucleases. For luciferase
621 reporter assays, HEK293 cells were plated at a density of 5x104 cells per well into 96-well

622 plates. 24 hours later, 50ng of transient expression vectors encoding either TAp63α or
623 ΔNp63α were transfected into these HEK293 cells either alone or alongside 50ng of the
624 firefly luciferase-expressing *pGL3-RHBDF2* vector or the positive control IRF6_BS2_p229
625 vector, in addition to 5ng of an internal control Renilla luciferase reporter vector, using
626 lipofectamine transfection reagent. After 24 more hours, lysates were collected by treating
627 with 20µl passive lysis buffer per well for 15 minutes. Luciferase was assayed by the Dual-
628 Luciferase system (Promega), with data presented as luciferase activity relative to
629 untransfected cells.

630 **RNA interference**

631 For p63 knockdown, siRNA sequences against TP63 (ID 217143, ID 4893 and ID 217144 from
632 Applied Biosystems) were used in combination to create a siRNA-p63 pool. For ADAM17
633 knockdown, siRNA sequences specific to against ADAM17 (L-003453-00-0005, OnTarget plus
634 SMARTPool ADAM17 siRNA, Dharmacon Lafayette, USA,). As a negative control, a non-
635 targeting siRNA pool (D-001810-10-20, ON-TARGETplus, Dharmacon Lafayette, USA) was
636 selected. Transfection was performed according to the manufacturer's protocol and
637 optimized for a six-well plate. Normal and TOC keratinocytes were plated at 50% confluency
638 and subjected to transfection on the following day using the transfection reagent Dharma
639 FECT 1 (Thermo Fisher Dharmacon) and 60 nM final concentration of each siRNA. During
640 siRNA application, antibiotics were removed from the cell culture medium. Transfection
641 media were replaced with complete DMEM after 24 h. p63 and ADAM17 expression were
642 assessed by western blot after 48 h.

643 **Immunoblot and co-immunoprecipitation**

644 After performing specific treatments, cells were harvested, washed three times with
645 phosphate-buffered saline (PBS) and then lysed using lysis buffer [1 M Tris, 2.5 M NaCl, 10%
646 glycerol, 0.5 M glycerophosphate, 1% Tween-20, 0.5% Nonidet P-40 and EDTA-free
647 Complete Protease Inhibitor tablet (Roche)] for 15 min on ice. Protein concentration was
648 measured using a Bradford Assay Kit (Bio-Rad). Equal amounts of protein were loaded and
649 separated by sodium dodecyl sulphate–polyacrylamide gel electrophoresis, SDS-PAGE (on
650 10% or 12% polyacrylamide gels) and transferred to a nitrocellulose membrane (Whatman).
651 The blots were incubated with the specific antibodies and developed according to the
652 manufacturer's instructions (ECL Immobilion Western, Millipore). Antibodies were diluted in
653 PBS containing 5% milk and 0.01% Tween 20. Co-immunoprecipitation experiments were
654 performed as previously described [12]. Briefly, the lysates were collected after 30 minutes
655 and pre-cleared by centrifugation at 13,000 rpm for 10 minutes at 4°C. Protein

656 concentration was calculated using the Bradford Protein Assay system (Bio-Rad). 50µl of
657 Sepharose protein G (Amersham) were prepared according to manufacturer's instructions.
658 IgG (Rabbit IgG sc-2027,) was used as a control. 2mg of protein lysate was added to beads
659 and antibodies (2µg) incubated overnight at 4°C with rotation. The following day beads were
660 washed three times for 5 minutes on ice in 1 ml of NP-40 wash buffer (50mM Tris pH 8.0,
661 150mM NaCl, 1mM EDTA, 1% NP40) containing protease and phosphatase inhibitors
662 (Roche). Beads were separated from antibody-protein complexes by boiling for 5 minutes in
663 2x Laemelli buffer and loaded onto a gel for SDS-PAGE electrophoresis. Uncut blots are
664 supplied in Supplementary Figure 6.

665 **qRT-PCR**

666 Total RNA was prepared with RNeasy mini Kit (Qiagen). cDNA was synthesized using High-
667 Capacity cDNA Reverse Transcription Kits strand (Thermo Scientific) for RT-PCR according to
668 the manufacturer's instructions. Semi-quantitative PCR was carried out using Maxima SYBR
669 Green/ROX qPCR master mix (Thermo Scientific, UK). Measurements were done in triplicate
670 and normalized to levels of GAPDH mRNA for each reaction and analysed using the equation
671 $n = 2^{-\Delta\Delta Ct}$. The following primers were used for qPCR analysis: for human genes *GAPDH*
672 forward 5'-GGAGTCAACGGATTTGGTC-3' and reverse 5'-GGCAACAATATCCACTTTACC-3';
673 *ΔNp63* forward 5'-GAGTTCTGTTATCTTCTTAG-3' and reverse 5'- TGTTCTGCGCGTGGTCTG-3';;
674 *HMOX1* forward 5'-AAAGTGCAAGATTCTGCCC-3' and reverse 5'- GAGTGTAAGGACCCATCGG-
675 3'; *NQO1* forward 5'- TCTATGCCATGAACTTCAATCC-3' and reverse 5'-
676 CTTCAGTTTACCTGTGATGTC-3'; *SOD1* forward 5'- GGATGAAGAGAGGCATGTTGGAGAC-3' and
677 reverse 5'- GTCTTTGTACTTTCTTCATTTCCACC-3'; *CYGB* forward 5'- CTGTCGTGGA
678 GAACCTGCAT-3' and 5'- TGGAGTTAGGGGTCCTACGG-3'; *RHBDF2* forward 5'-
679 GGGCAAACTCAGACTCGAAG-3' and reverse 5'- CGCTGACTCCAAACCACTG-3', *ADAM17*
680 forward 5'- GGTTCCTTTCGTGCTGGCGC-3' and reverse 5'- AAGCTTCTCGAGTCTCTGGTGGG-3';
681 *NRF2* forward 5'- CAGCGACGGAAAGAGTATGA-3' and reverse 5'-TGGGCAACCTGGGAGTAG-
682 3'. For mouse genes *ΔNp63* forward 5'- GTACCTGGAAAACAATGCCCAG-3' and reverse 5'-
683 CGCTATTCTGTGCCTGGTCTG-3'; GAPDH forward 5'- ACCACAGTCCATGCCATCAC-3' and
684 reverse 5'- TCCACCACCCTGTTGCTGTA-3'.

685 **The enzyme-linked immunosorbent assay (ELISA)**

686 After performing specific treatments, cell culture supernatants were used to detect TNF-α,
687 IL-6R and TGF-α by ELISA using the human DuoSet ELISA kit as to the manufacturer's

688 instructions (R&D System, UK). Results were expressed as means of four independent
689 experiments with triplicate samples.

690 **Immunofluorescence**

691 Immunohistochemistry was performed on 5 mm frozen tissue or on cells plated in cover
692 slips; sections were air-dried before processed. Cells/tissues were fixed in 4%
693 paraformaldehyde (PFA) or in ice cold Methanol-Acetone (50:50 mixture) at room
694 temperature for 15 min. If PFA fixation was used, samples were permeabilized with 0.1%
695 Triton X-100. Cells/tissues were washed three times with PBS for 5 min each and incubated
696 with 5% goat serum in PBS for 1 hour at room temperature to reduce nonspecific binding.
697 After the cells/tissue were incubated with primary antibody in 5% goat serum overnight at
698 4˚C. The following day cells/tissues were washed three times with PBS and incubated with
699 the secondary antibody conjugated with Alexa Fluor (Molecular Probes) in 5% goat serum
700 for 1 h at room temperature. After three washes, cells/sections were incubated for 10 min
701 with DAPI (100 ng/ml). Cells/tissues were mounted onto slides using Vectashield Mounting
702 Medium (Vector Laboratories). Fluorescence was evaluated in one single plane by Zeiss 710
703 confocal microscopy (Carl Zeiss).

704 **Haematoxylin and Eosin (H&E)**

705 Tissue sections were fixed in 4% PFA and stained with haematoxylin and eosin.

706

707 **Cell proliferation**

708 To analyse cell proliferation after performing transfection with siRNA, cells were plated at a
709 seeding density of $1x10^4$ per well and then harvested at 24 and 48 h. For SFN exposure, cells
710 were seeded at $1x10^4$ per well and then treated with SFN at 10 µM. Cells were counted after
711 24 and 48 hours post treatment. Cell counts were performed using the
712 Nucleocounter/Nucleocasette system (ChemoMetec, Denmark). Each experiment was
713 repeated three times with triplicate samples.

714 **Scratch assay**

715 Cells were seeded into six-well plates in culture medium and were transfected with siRNA.
716 The cells were incubated with mitomycin C (400 ng ml^{-1}, Roche) for 45 min to prevent
717 proliferation. The scratch wound was created vertically to the centre of the well using a

718 sterile tip to 200 µl. The cells were subsequently washed with PBS to remove the detached
719 cells and then replenished with fresh medium. The woundwas monitored and
720 photographed immediately (time 0) and after 24 h from the creation of the scratch using a
721 phase-contrast microscope. The wound area was evaluated by using Image J Software. The
722 percentage was calculated using the following equation: [Wound Area (0h) - Wound Area
723 (Xh)] x 100 /Wound Area (0h) = % Wound Closure.

724 **Annexin V assay**

725 Apoptosis was assessed by flow cytometry using FITC Annexin-V (Becton Dickinson) and
726 DAPI. The cells were harvested by the addition of trypsin, centrifuged for 5 min at 1200 rpm,
727 and washed with PBS. Cells were stained with FITC-Annexin V for 15 minutes and the DAPI
728 (200 ng/ml) was added. Samples were analysed by a BD FACSCanto II Flow Cytometer (BD,
729 UK). Data were expressed as means of total apoptosis, the sum of early and late apoptosis.
730 The gating strategy is reported in Supplementary Fig.7.

731 **Proximity ligation assay (PLA)**

732 PLA was performed using the Duolink in situ kit (Sigma) according to the manufacturer's
733 instructions. Cells were plated on coverslips in twelve-well plates and after 24 h fixed with
734 Methanol Acetone or PFA. Following fixation, cells were incubated in Duolink blocking
735 solution for 30 min at 37°C. Primary antibodies were diluted in Duolink Antibody diluent and
736 added to the cells overnight at 4°C. The following day the cells were washed in Wash buffer
737 A two times for 5 min. The PLA plus and minus probes were diluted in antibody diluent and
738 added to the cells, then incubated for 1 h at 37°C. The cells were washed in Wash buffer A
739 two times for 5 min. The Ligation–Ligase was prepared according to instructions and applied
740 to cells for 30 min at 37°C. After washes, amplification with Duolink Amplification-
741 Polymerase solution was performed for 100 min at 37°C. The cells were washed in Wash
742 Buffer B two times for 10 min and then mounted with Duolink in situ mounting medium
743 with DAPI before visualization with Zeiss 710 confocal microscopy (Carl Zeiss). As a positive
744 control binding between K6 and K16 was analysed, while as a negative control no primary
745 antibodies were applied. Quantifications were performed using Image J Software.

746 **Measurement of ROS Production**

747 The quantification of intracellular ROS was based on the oxidation of dihydroethidium (DHE,
748 Thermo Fisher). Briefly, normal and TOC keratinocytes ($2x10^5$) were plated in each well of 6-

749 well plate. Cells were then washed twice with PBS and incubated with DHE (5µM) at 37°C
750 for 30 min in the dark. After incubation, the cell were washed twice with PBS and were
751 analysed by a BD FACSCanto II Flow Cytometer (BD, UK). Data represented the value of ROS
752 in the live cells by a ratio referred to the control. For staining, normal and TOC keratinocytes
753 ($5x10^4$) were plated on cover slip in each well of 12-well plate. The cells on cover slip were
754 washed twice with HBSS after exposure to DHE (Thermo Scientific) working concentration
755 (5µM) at 37 °C for 30 min in the dark. Before microscopy, Hoechst® 33342 (0.1 µg/ml,
756 Thermo Scientific) was added to stain the nuclei. The fluorescence was analysed using Zeiss
757 710 confocal microscopy (Carl Zeiss).

758 **Mouse studies**

759 *rhbdf2*$^{-/-}$ mice were generated as previously described [12]. The fore paw footpad epidermis
760 from twenty-week-old *rhbdf2*$^{-/-}$ or WT female mice were dissected and fixed in OCT on dry
761 ice. Immunohistochemical staining was performed as previously described and visualized
762 using the Zeiss 710 Confocal Microscope (Carl Zeiss). Biopsies from WT female mice (n=6 per
763 genotype, back and paw skin) were snap frozen, pulverized, and dissolved in TRIzol reagent
764 for RNA preparation (Invitrogen) according to manufacturer's protocol. RNA samples were
765 treated with RNase-free DNaseI (Qiagen). Western blot analysis of mouse skin extract were
766 prepared in urea buffer 8M (8M urea, 1M thiourea, 0.5% CHAPS, 50 mM DTT, 24 mM
767 spermine).

768 **Study approval**

769 All experiments involving mice followed the UK Animal Welfare Act guidelines and were
770 approved by the UK Home Office (PPL 70/7665). Human skin biopsies were approved by the
771 research ethics committees of the National Health Service (08/H1102/73) and informed
772 consent was obtained from participants.

773 **Statistical analysis**

774 All statistical analyses were performed with Prism 6 Software (GraphPad). Data were
775 analysed by the unpaired/paired two-tailed Student's t test and one way ANOVA Dunnett's
776 multiple comparison test. All experiments were performed at least three times
777 independently or more indicated in the legends. The data are expressed as the mean ±
778 standard error of mean (SEM).

779 [$p < 0.05$ (*), $p < 0.01$ (**) and $p < 0.001$ (***)]

Acknowledgements

We would like to thank Prof Nick Reynolds and Dr Richard Grose for critical reading of the manuscript. We are grateful to Dr Eleonora Candi for providing constructs. We would like to thank Dr Gary Warnes, Flow Cytometry Core Facility Manager for technical advice; Dr Belén Martín-Martín and Dr Jan Soetaert, Microscopy facility for assistance with the confocal microscopy and Rebecca Carroll (BMS2) core Pathology laboratory for technical support with tissue samples. The study was supported by grants awarded to DPK from the Medical Research Council (MR/L010402/1), Cancer Research UK (C7570/A19107), the 2016 CHANEL-CERIES research award and the British Heart Foundation (RG/13/19/30568). The fellowship awarded to PA was from the European Commission and Regione UMBRIA under grant agreement FP7 Marie Curie Actions COFUND, I-MOVE (267232). The authors declare no competing financial interests.

Data availability

The data that support the findings of this study are available from the corresponding authors (D.P.K., A.C.) upon reasonable request.

References

1 Maruthappu, T., Scott, C. A. & Kelsell, D. P. Discovery in genetic skin disease: the impact of high throughput genetic technologies. *Genes* **5**, 615-634, doi:10.3390/genes5030615 (2014).

2 Blaydon, D. C. & Kelsell, D. P. Defective channels lead to an impaired skin barrier. *Journal of Cell Science* **127**, 4343-4350, doi:10.1242/jcs.154633 (2014).

3 Blaydon, Diana C. *et al.* RHBDF2 Mutations Are Associated with Tylosis, a Familial Esophageal Cancer Syndrome. *American Journal of Human Genetics* **90**, 340-346, doi:10.1016/j.ajhg.2011.12.008 (2012).

4 Kelsell, D. P., Di, W.-L. & Houseman, M. J. Connexin Mutations in Skin Disease and Hearing Loss. *American Journal of Human Genetics* **68**, 559-568 (2001).

5 Blaydon, D. C. *et al.* RHBDF2 mutations are associated with tylosis, a familial esophageal cancer syndrome. *American journal of human genetics* **90**, 340-346, doi:10.1016/j.ajhg.2011.12.008 (2012).

814 6 Lemberg, M. K. & Freeman, M. Cutting proteins within lipid bilayers: rhomboid
815 structure and mechanism. *Molecular cell* **28**, 930-940,
816 doi:10.1016/j.molcel.2007.12.003 (2007).
817 7 Adrain, C., Zettl, M., Christova, Y., Taylor, N. & Freeman, M. Tumor necrosis factor
818 signaling requires iRhom2 to promote trafficking and activation of TACE. *Science* **335**,
819 225-228, doi:10.1126/science.1214400 (2012).
820 8 Maretzky, T. *et al.* iRhom2 controls the substrate selectivity of stimulated ADAM17-
821 dependent ectodomain shedding. *Proceedings of the National Academy of Sciences*
822 *of the United States of America* **110**, 11433-11438, doi:10.1073/pnas.1302553110
823 (2013).
824 9 Brooke, M. A. *et al.* iRHOM2-dependent regulation of ADAM17 in cutaneous disease
825 and epidermal barrier function. *Human molecular genetics* **23**, 4064-4076,
826 doi:10.1093/hmg/ddu120 (2014).
827 10 Grieve, A. G. *et al.* Phosphorylation of iRhom2 at the plasma membrane controls
828 mammalian TACE-dependent inflammatory and growth factor signalling. *eLife* **6**,
829 doi:10.7554/eLife.23968 (2017).
830 11 Gooz, M. ADAM-17: the enzyme that does it all. *Critical reviews in biochemistry and*
831 *molecular biology* **45**, 146-169, doi:10.3109/10409231003628015 (2010).
832 12 Maruthappu, T. *et al.* Rhomboid family member 2 regulates cytoskeletal stress-
833 associated Keratin 16. *Nature communications* **8**, 14174, doi:10.1038/ncomms14174
834 (2017).
835 13 Yang, A. *et al.* p63, a p53 homolog at 3q27-29, encodes multiple products with
836 transactivating, death-inducing, and dominant-negative activities. *Molecular cell* **2**,
837 305-316 (1998).
838 14 Mills, A. A. *et al.* p63 is a p53 homologue required for limb and epidermal
839 morphogenesis. *Nature* **398**, 708-713, doi:10.1038/19531 (1999).
840 15 Yang, X. *et al.* DeltaNp63 versatilely regulates a Broad NF-kappaB gene program and
841 promotes squamous epithelial proliferation, migration, and inflammation. *Cancer*
842 *research* **71**, 3688-3700, doi:10.1158/0008-5472.CAN-10-3445 (2011).
843 16 Missero, C. & Antonini, D. p63 in Squamous Cell Carcinoma of the Skin: More Than a
844 Stem Cell/Progenitor Marker. *The Journal of investigative dermatology* **137**, 280-281,
845 doi:10.1016/j.jid.2016.10.032 (2017).
846 17 Romano, R. A., Smalley, K., Liu, S. & Sinha, S. Abnormal hair follicle development and
847 altered cell fate of follicular keratinocytes in transgenic mice expressing
848 DeltaNp63alpha. *Development* **137**, 1431-1439, doi:10.1242/dev.045427 (2010).
849 18 Rizzo, J. M. *et al.* DeltaNp63 regulates IL-33 and IL-31 signaling in atopic dermatitis.
850 *Cell death and differentiation* **23**, 1073-1085, doi:10.1038/cdd.2015.162 (2016).
851 19 Kouwenhoven, E. N. *et al.* Genome-wide profiling of p63 DNA-binding sites identifies
852 an element that regulates gene expression during limb development in the 7q21
853 SHFM1 locus. *PLoS genetics* **6**, e1001065, doi:10.1371/journal.pgen.1001065 (2010).
854 20 Sethi, I., Gluck, C., Zhou, H., Buck, M. J. & Sinha, S. Evolutionary re-wiring of p63 and
855 the epigenomic regulatory landscape in keratinocytes and its potential implications
856 on species-specific gene expression and phenotypes. *Nucleic acids research* **45**, 8208-
857 8224, doi:10.1093/nar/gkx416 (2017).
858 21 Chikh, A. *et al.* iASPP/p63 autoregulatory feedback loop is required for the
859 homeostasis of stratified epithelia. *The EMBO journal* **30**, 4261-4273,
860 doi:10.1038/emboj.2011.302 (2011).

861 22 Ellis, A., Risk, J. M., Maruthappu, T. & Kelsell, D. P. Tylosis with oesophageal cancer:
862 Diagnosis, management and molecular mechanisms. *Orphanet journal of rare*
863 *diseases* **10**, 126, doi:10.1186/s13023-015-0346-2 (2015).
864 23 Lee, H. O., Lee, J. H., Kim, T. Y. & Lee, H. Regulation of DeltaNp63alpha by tumor
865 necrosis factor-alpha in epithelial homeostasis. *The FEBS journal* **274**, 6511-6522,
866 doi:10.1111/j.1742-4658.2007.06168.x (2007).
867 24 Nakanishi, G., Kim, Y. S., Nakajima, T. & Jetten, A. M. Regulatory role for Kruppel-like
868 zinc-finger protein Gli-similar 1 (Glis1) in PMA-treated and psoriatic epidermis. *The*
869 *Journal of investigative dermatology* **126**, 49-60, doi:10.1038/sj.jid.5700018 (2006).
870 25 Younus, J. & Gilchrest, B. A. Modulation of mRNA levels during human keratinocyte
871 differentiation. *Journal of cellular physiology* **152**, 232-239,
872 doi:10.1002/jcp.1041520203 (1992).
873 26 Inoue, S. *et al.* TAp73 is required for spermatogenesis and the maintenance of male
874 fertility. *Proceedings of the National Academy of Sciences of the United States of*
875 *America* **111**, 1843-1848, doi:10.1073/pnas.1323416111 (2014).
876 27 Mirza, A. *et al.* Human survivin is negatively regulated by wild-type p53 and
877 participates in p53-dependent apoptotic pathway. *Oncogene* **21**, 2613-2622,
878 doi:10.1038/sj.onc.1205353 (2002).
879 28 Kerns, M. L. *et al.* Oxidative stress and dysfunctional NRF2 underlie pachyonychia
880 congenita phenotypes. *The Journal of clinical investigation* **126**, 2356-2366,
881 doi:10.1172/JCI84870 (2016).
882 29 Biswas, S. K. Does the Interdependence between Oxidative Stress and Inflammation
883 Explain the Antioxidant Paradox? *Oxidative medicine and cellular longevity* **2016**,
884 5698931, doi:10.1155/2016/5698931 (2016).
885 30 Halliwell, B. Oxidative stress and cancer: have we moved forward? *The Biochemical*
886 *journal* **401**, 1-11, doi:10.1042/BJ20061131 (2007).
887 31 Latina, A. *et al.* DeltaNp63 targets cytoglobin to inhibit oxidative stress-induced
888 apoptosis in keratinocytes and lung cancer. *Oncogene* **35**, 1493-1503,
889 doi:10.1038/onc.2015.222 (2016).
890 32 Hodges, N. J., Innocent, N., Dhanda, S. & Graham, M. Cellular protection from
891 oxidative DNA damage by over-expression of the novel globin cytoglobin in vitro.
892 *Mutagenesis* **23**, 293-298, doi:10.1093/mutage/gen013 (2008).
893 33 Fordel, E., Thijs, L., Moens, L. & Dewilde, S. Neuroglobin and cytoglobin expression in
894 mice. Evidence for a correlation with reactive oxygen species scavenging. *The FEBS*
895 *journal* **274**, 1312-1317, doi:10.1111/j.1742-4658.2007.05679.x (2007).
896 34 Gardner, A. M., Cook, M. R. & Gardner, P. R. Nitric-oxide dioxygenase function of
897 human cytoglobin with cellular reductants and in rat hepatocytes. *The Journal of*
898 *biological chemistry* **285**, 23850-23857, doi:10.1074/jbc.M110.132340 (2010).
899 35 McRonald, F. E. *et al.* Down-regulation of the cytoglobin gene, located on 17q25, in
900 tylosis with oesophageal cancer (TOC): evidence for trans-allele repression. *Human*
901 *molecular genetics* **15**, 1271-1277, doi:10.1093/hmg/ddl042 (2006).
902 36 McRonald, F. E., Risk, J. M. & Hodges, N. J. Protection from intracellular oxidative
903 stress by cytoglobin in normal and cancerous oesophageal cells. *PloS one* **7**, e30587,
904 doi:10.1371/journal.pone.0030587 (2012).
905 37 Toivola, D. M., Zhou, Q., English, L. S. & Omary, M. B. Type II keratins are
906 phosphorylated on a unique motif during stress and mitosis in tissues and cultured

907 cells. *Molecular biology of the cell* **13**, 1857-1870, doi:10.1091/mbc.01-12-0591
908 (2002).
909 38 Ambrosini, G., Adida, C. & Altieri, D. C. A novel anti-apoptosis gene, survivin,
910 expressed in cancer and lymphoma. *Nature medicine* **3**, 917-921 (1997).
911 39 Carroll, D. K. *et al.* p63 regulates an adhesion programme and cell survival in
912 epithelial cells. *Nature cell biology* **8**, 551-561, doi:10.1038/ncb1420 (2006).
913 40 Liefer, K. M. *et al.* Down-regulation of p63 is required for epidermal UV-B-induced
914 apoptosis. *Cancer research* **60**, 4016-4020 (2000).
915 41 Lotti, R. *et al.* Survivin Modulates Squamous Cell Carcinoma-Derived Stem-Like Cell
916 Proliferation, Viability and Tumor Formation in Vivo. *International journal of*
917 *molecular sciences* **17**, doi:10.3390/ijms17010089 (2016).
918 42 Chakraborty, S., John, R. & Nag, A. Cytoglobin in tumor hypoxia: novel insights into
919 cancer suppression. *Tumour biology : the journal of the International Society for*
920 *Oncodevelopmental Biology and Medicine* **35**, 6207-6219, doi:10.1007/s13277-014-
921 1992-z (2014).
922 43 Tortorella, S. M., Royce, S. G., Licciardi, P. V. & Karagiannis, T. C. Dietary
923 Sulforaphane in Cancer Chemoprevention: The Role of Epigenetic Regulation and
924 HDAC Inhibition. *Antioxidants & redox signaling* **22**, 1382-1424,
925 doi:10.1089/ars.2014.6097 (2015).
926 44 Fimognari, C. *et al.* Sulforaphane modulates cell cycle and apoptosis in transformed
927 and non-transformed human T lymphocytes. *Annals of the New York Academy of*
928 *Sciences* **1010**, 393-398 (2003).
929 45 Thimmulappa, R. K. *et al.* Identification of Nrf2-regulated genes induced by the
930 chemopreventive agent sulforaphane by oligonucleotide microarray. *Cancer research*
931 **62**, 5196-5203 (2002).
932 46 Guerrero-Beltran, C. E., Calderon-Oliver, M., Pedraza-Chaverri, J. & Chirino, Y. I.
933 Protective effect of sulforaphane against oxidative stress: recent advances.
934 *Experimental and toxicologic pathology : official journal of the Gesellschaft fur*
935 *Toxikologische Pathologie* **64**, 503-508, doi:10.1016/j.etp.2010.11.005 (2012).
936 47 Heiss, E., Herhaus, C., Klimo, K., Bartsch, H. & Gerhauser, C. Nuclear factor kappa B is
937 a molecular target for sulforaphane-mediated anti-inflammatory mechanisms. *The*
938 *Journal of biological chemistry* **276**, 32008-32015, doi:10.1074/jbc.M104794200
939 (2001).
940 48 Juge, N., Mithen, R. F. & Traka, M. Molecular basis for chemoprevention by
941 sulforaphane: a comprehensive review. *Cellular and molecular life sciences : CMLS*
942 **64**, 1105-1127, doi:10.1007/s00018-007-6484-5 (2007).

943

944 **Contributions**

945 P.A., D.P.K. and A.C. designed the research study. P.A., C.W, M.A.B and A.C. performed the
946 experiments and the analysis of the data. H.Z provided the ChIP-seq data sets and their
947 analysis. D.B provided the human tissue slides. P.J.D, K.E.N, A.T provided the mouse
948 samples. P.A., D.P.K. and A.C wrote the manuscript.

949 **Competing Financial interests**

The authors declare no competing financial interest.

Fig. 1

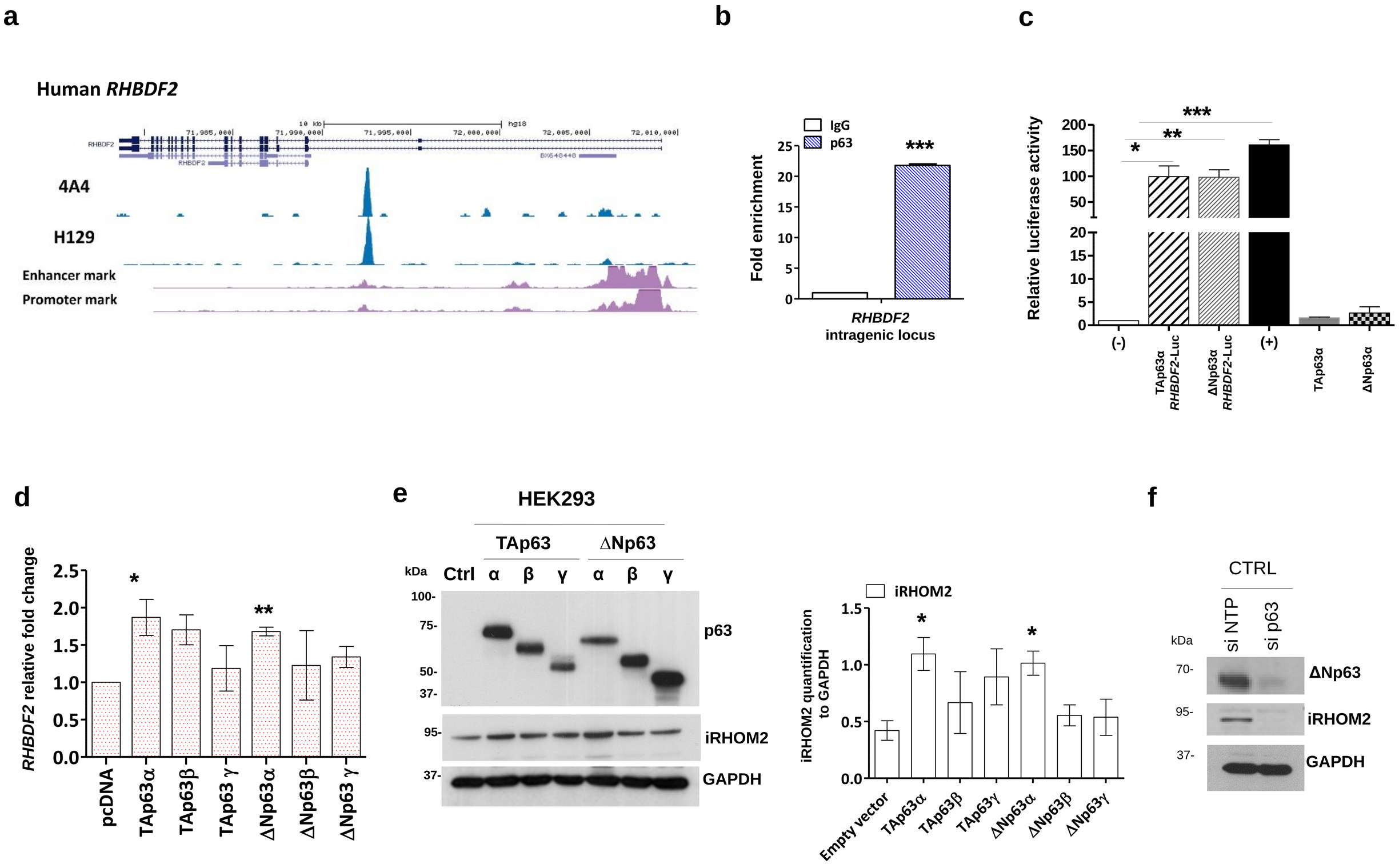
a
Human RHBDF2
RHBDF2
4A4
H129
Enhancer mark
Promoter mark
b
IgG
p63
Fold enrichment
RHBDF2
intragenic locus
c
Relative luciferase activity
(-)
TAp63α RHBDF2-Luc
ΔNp63α RHBDF2-Luc
(+)
TAp63α
ΔNp63α
d
RHBDF2 relative fold change
pcDNA
TAp63α
TAp63β
TAp63 γ
ΔNp63α
ΔNp63β
ΔNp63 γ
e
HEK293
TAp63
ΔNp63
kDa
Ctrl
α
β
γ
p63
iRHOM2
GAPDH
iRHOM2 quantification to GAPDH
Empty vector
f
CTRL
si NTP
si p63
ΔNp63
iRHOM2
GAPDH

Fig. 2

a

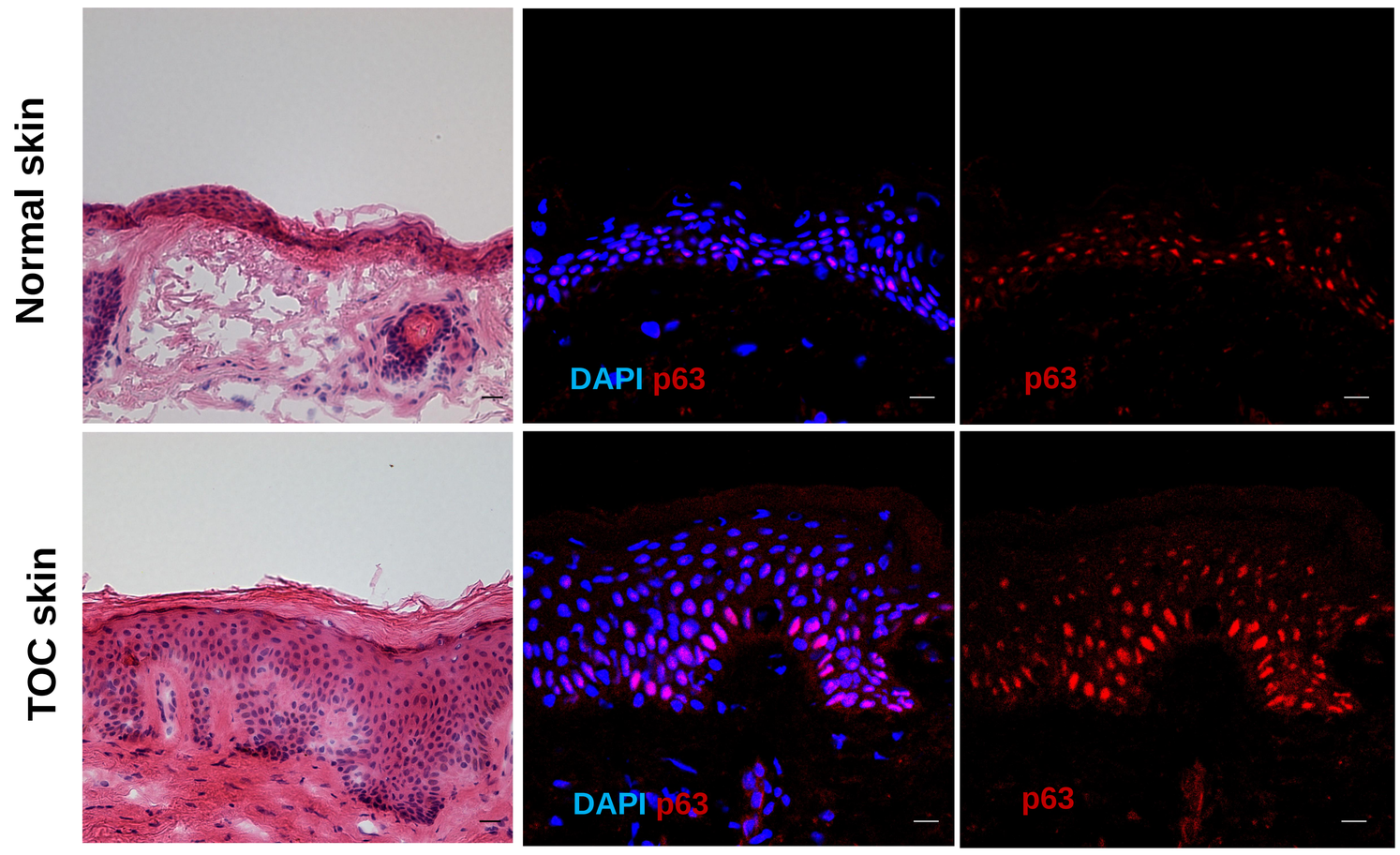
Normal skin
TOC skin
DAPI p63
p63
DAPI p63
p63

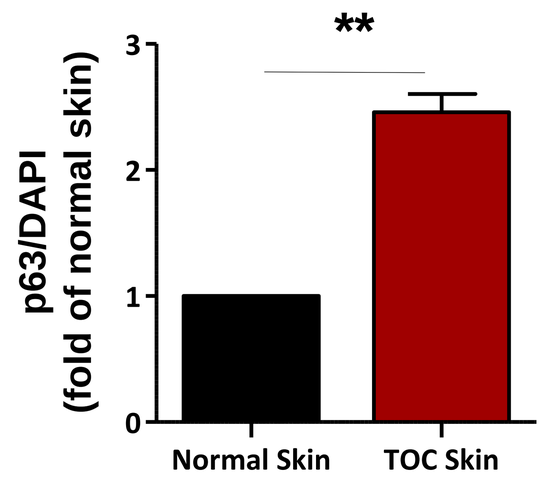
**
p63/DAPI
(fold of normal skin)
3
2
1
0
Normal Skin
TOC Skin

b

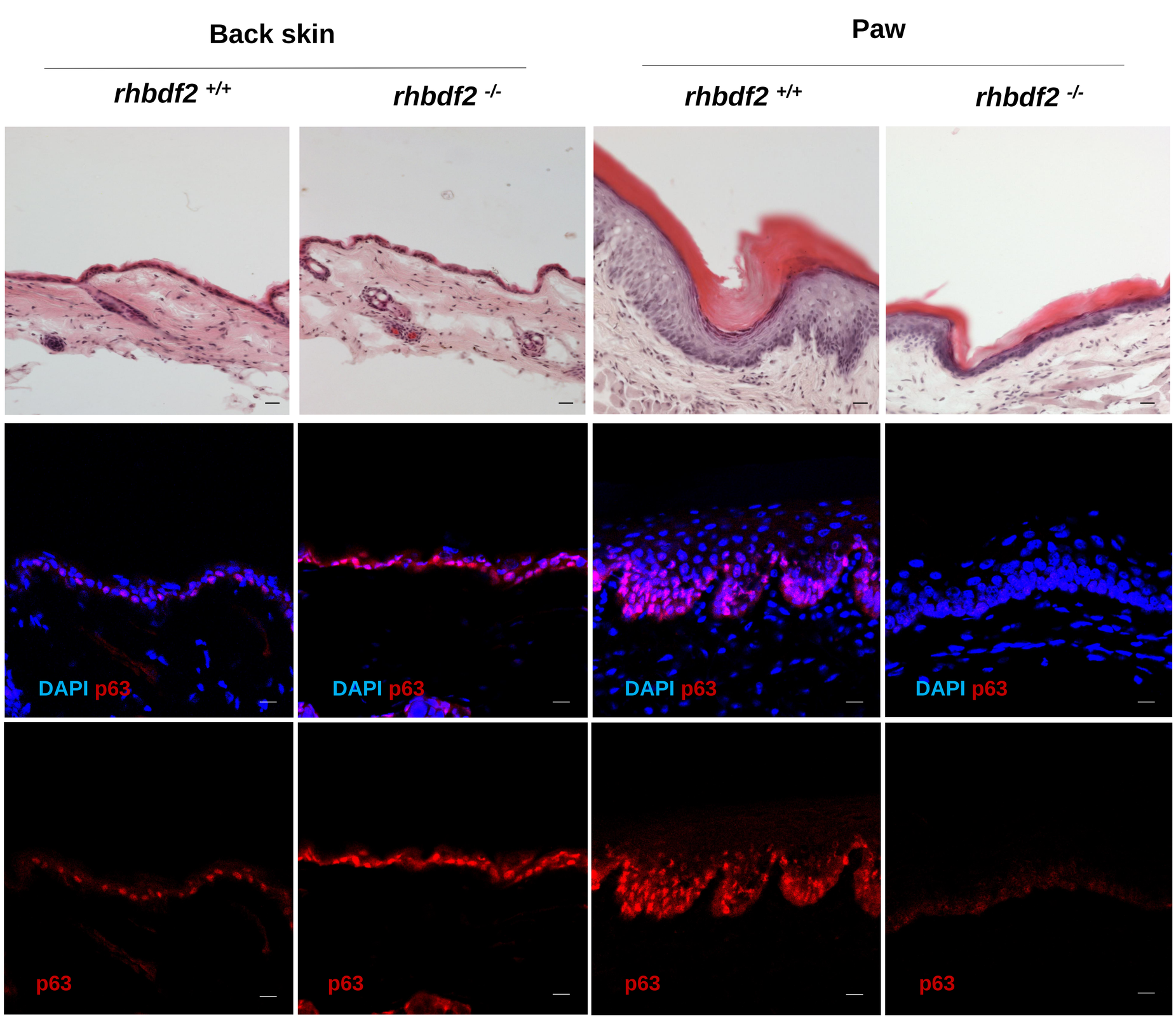
Back skin
Paw
rhbdf2 +/+
rhbdf2 -/-
rhbdf2 +/+
rhbdf2 -/-
DAPI p63
p63

c

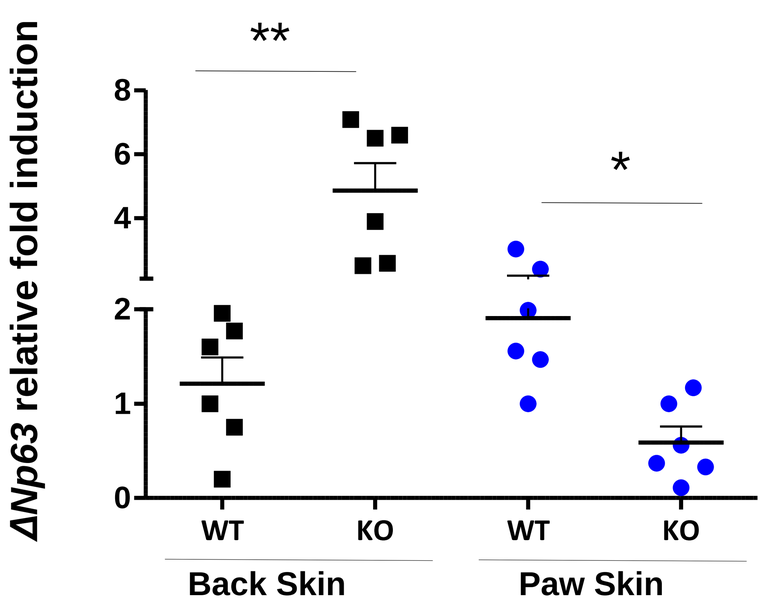
ΔNp63 relative fold induction
**
*
8
6
4
2
1
0
WT
KO
WT
KO
Back Skin
Paw Skin

Fig. 3

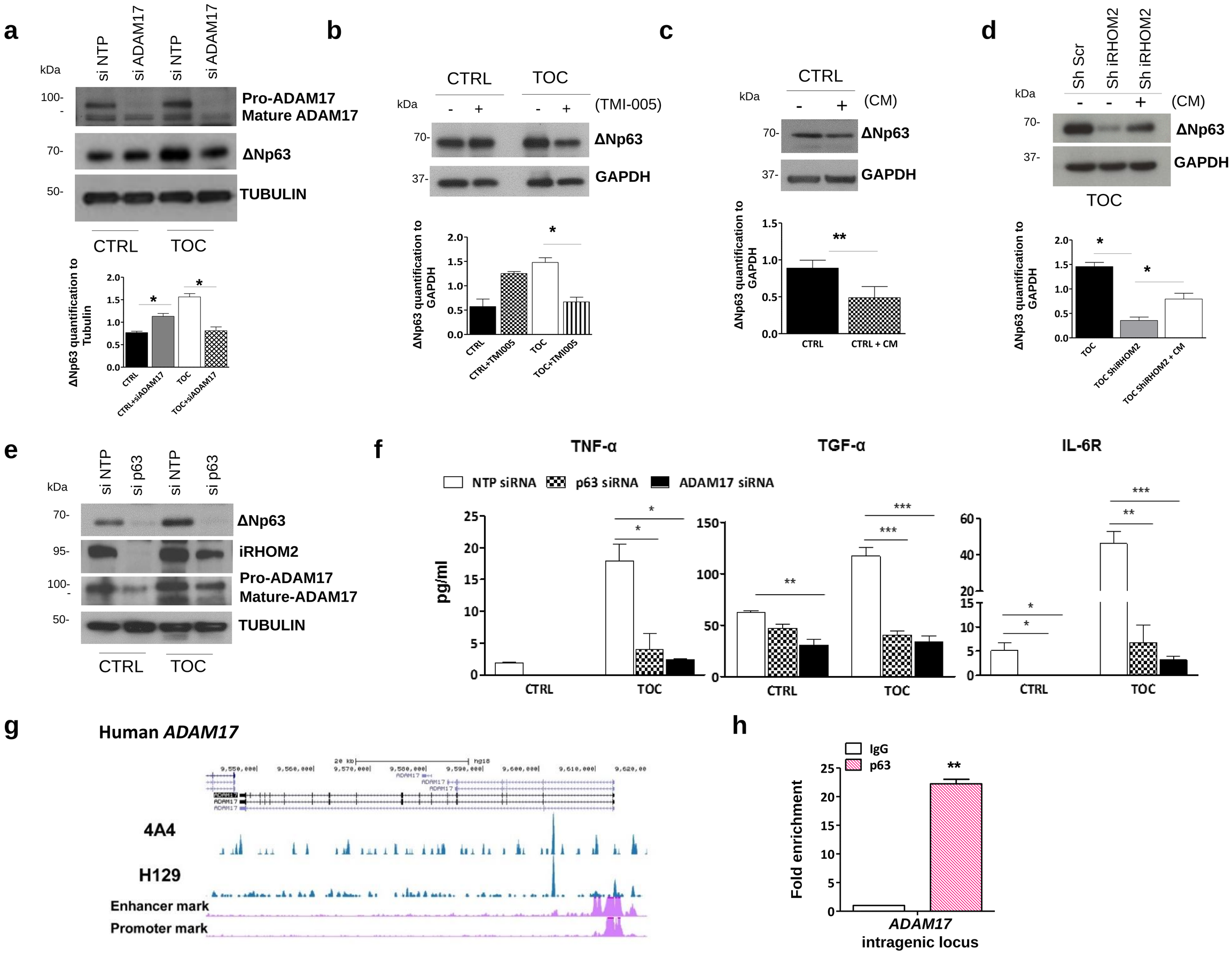
a
si NTP
si ADAM17
si NTP
si ADAM17
kDa
100-
Pro-ADAM17
Mature ADAM17
70-
ΔNp63
50-
TUBULIN
CTRL
TOC
ΔNp63 quantification to Tubulin
CTRL
CTRL+siADAM17
TOC
TOC+siADAM17
b
CTRL
TOC
kDa
(TMI-005)
70-
ΔNp63
37-
GAPDH
ΔNp63 quantification to GAPDH
CTRL
CTRL+TMI005
TOC
TOC+TMI005
c
CTRL
kDa
(CM)
70-
ΔNp63
37-
GAPDH
ΔNp63 quantification to GAPDH
CTRL
CTRL + CM
d
Sh Scr
Sh iRHOM2
Sh iRHOM2
kDa
(CM)
70-
ΔNp63
37-
GAPDH
TOC
ΔNp63 quantification to GAPDH
TOC
TOC ShiRHOM2
TOC ShiRHOM2 + CM
e
si NTP
si p63
si NTP
si p63
kDa
70-
ΔNp63
95-
iRHOM2
100-
Pro-ADAM17
Mature-ADAM17
50-
TUBULIN
CTRL
TOC
f
TNF-α
TGF-α
IL-6R
NTP siRNA
p63 siRNA
ADAM17 siRNA
pg/ml
CTRL
TOC
g
Human ADAM17
4A4
H129
Enhancer mark
Promoter mark
h
IgG
p63
Fold enrichment
ADAM17
intragenic locus

Fig. 4

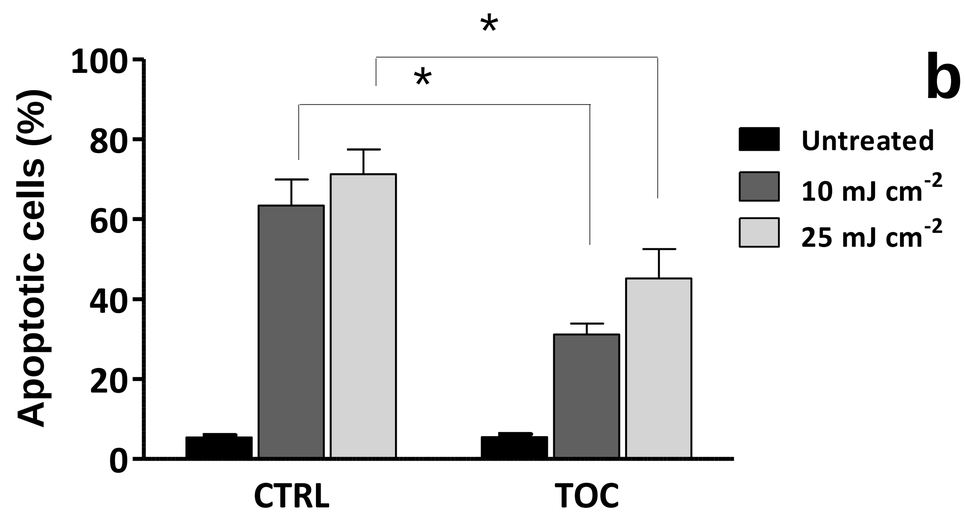
a
Apoptotic cells (%)
100
80
60
40
20
0
*
*
CTRL
TOC
Untreated
10 mJ cm-2
25 mJ cm-2

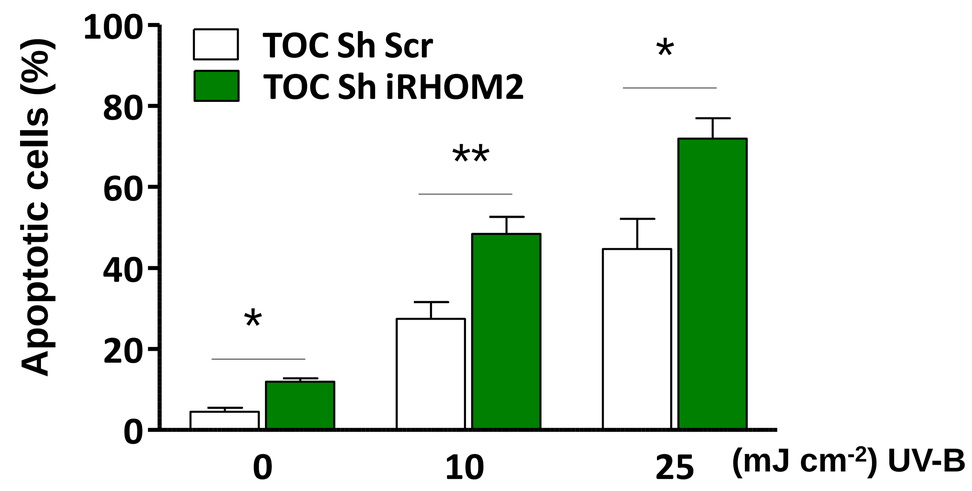
b
Apoptotic cells (%)
100
80
60
40
20
0
TOC Sh Scr
TOC Sh iRHOM2
*
**
*
0
10
25
(mJ cm-2) UV-B

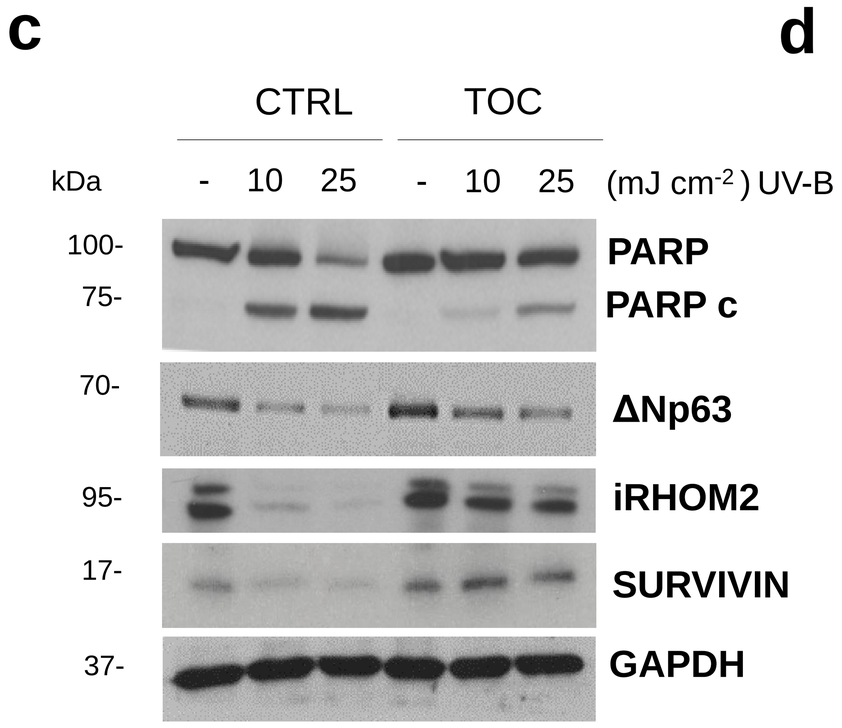
c
CTRL
TOC
kDa
- 10 25 - 10 25 (mJ cm-2) UV-B
100-
75-
PARP
PARP c
70-
ΔNp63
95-
iRHOM2
17-
SURVIVIN
37-
GAPDH

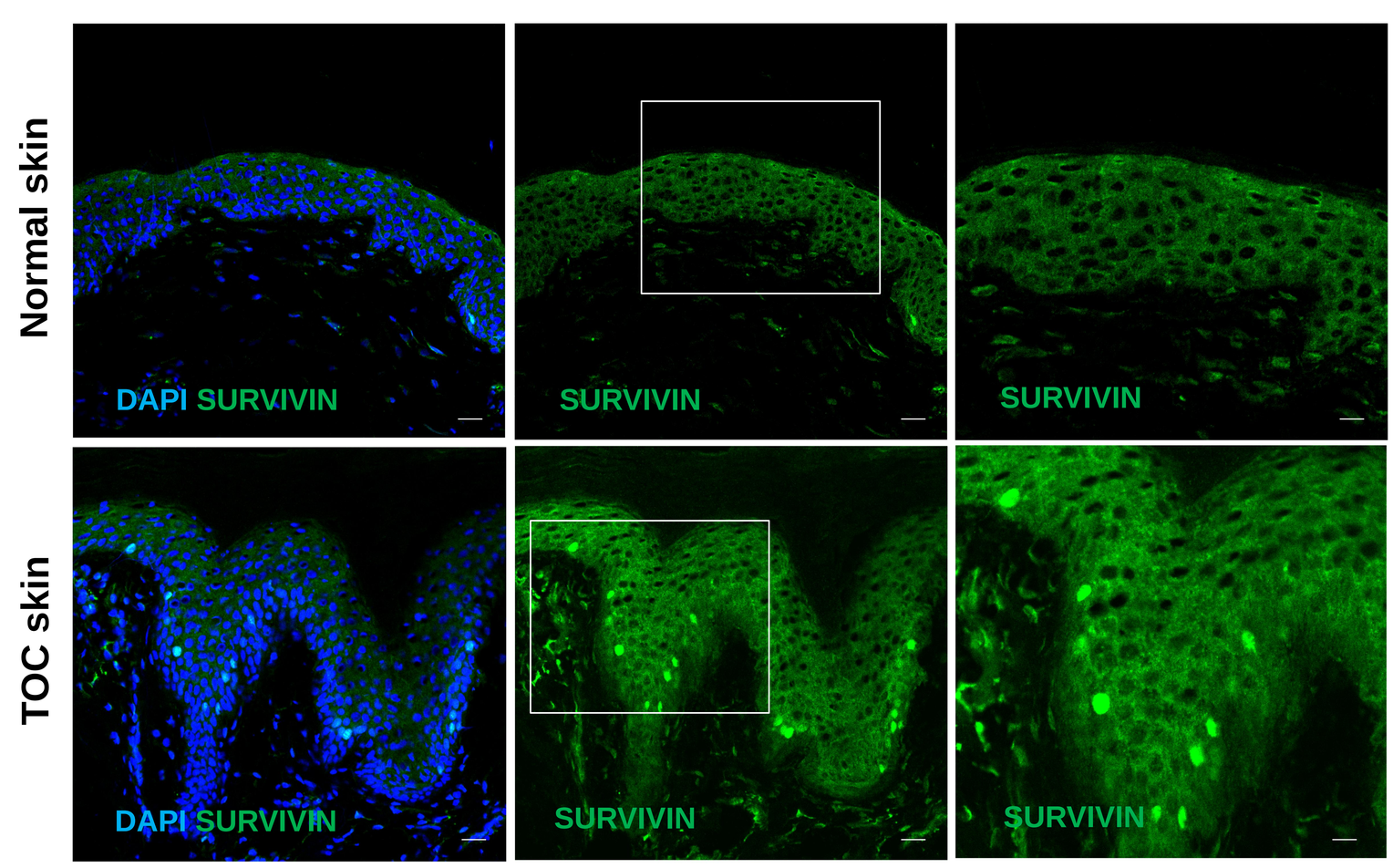
d
Normal skin
TOC skin
DAPI SURVIVIN
SURVIVIN
SURVIVIN
DAPI SURVIVIN
SURVIVIN
SURVIVIN

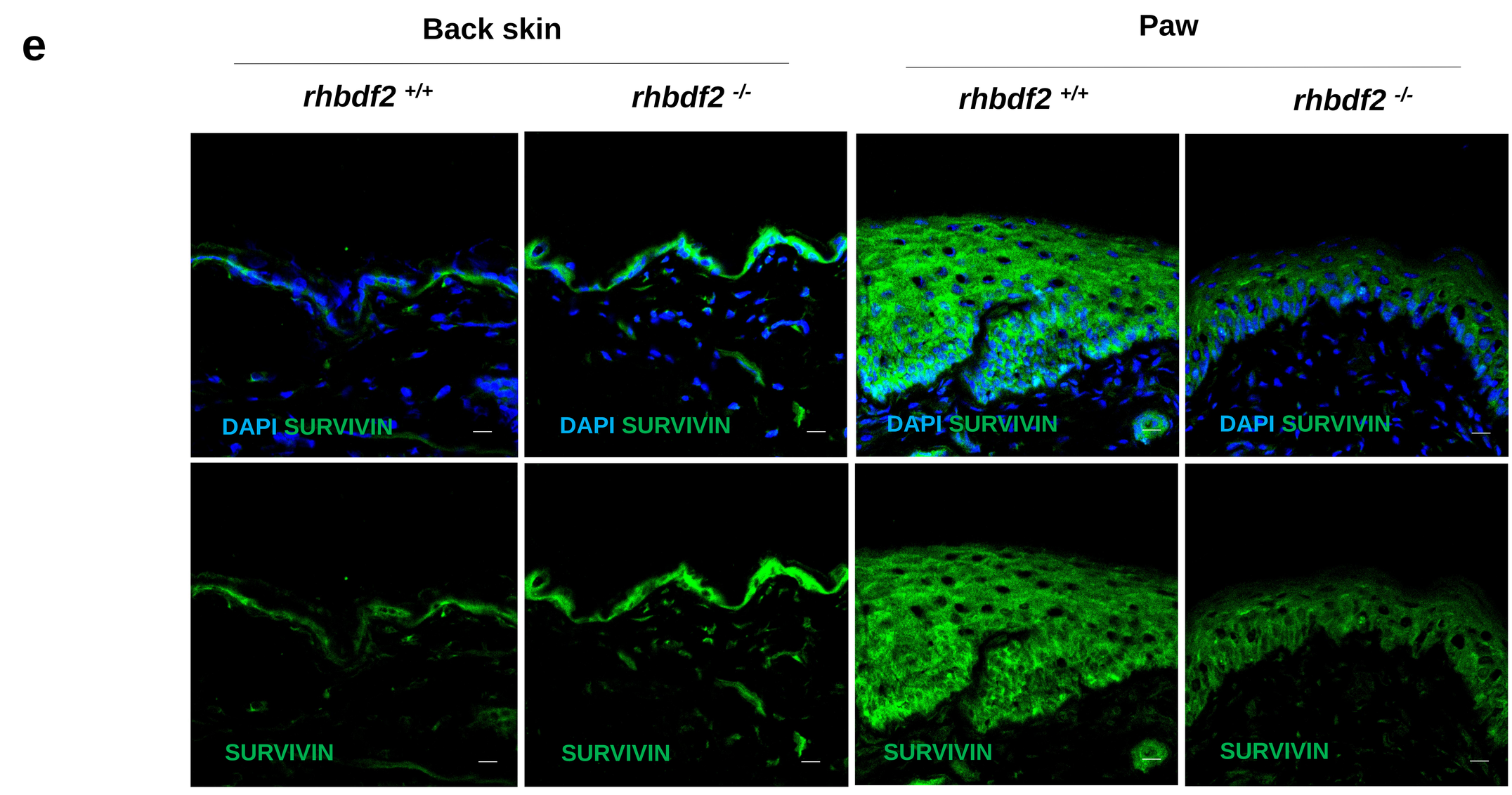
e
Back skin
Paw
rhbdf2 +/+
rhbdf2 -/-
rhbdf2 +/+
rhbdf2 -/-
DAPI SURVIVIN
DAPI SURVIVIN
DAPI SURVIVIN
DAPI SURVIVIN
SURVIVIN
SURVIVIN
SURVIVIN
SURVIVIN

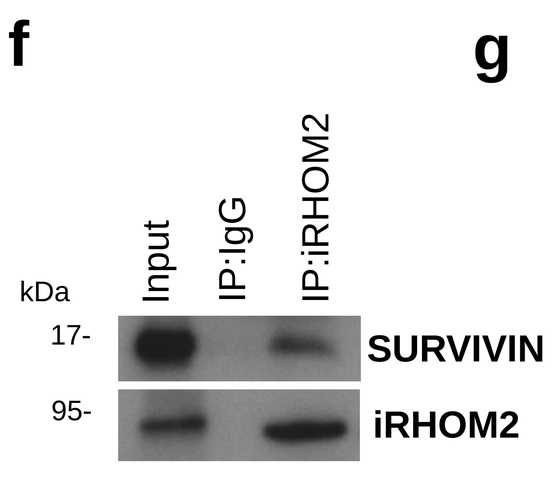
f
kDa
Input
IP:IgG
IP:iRHOM2
17-
SURVIVIN
95-
iRHOM2

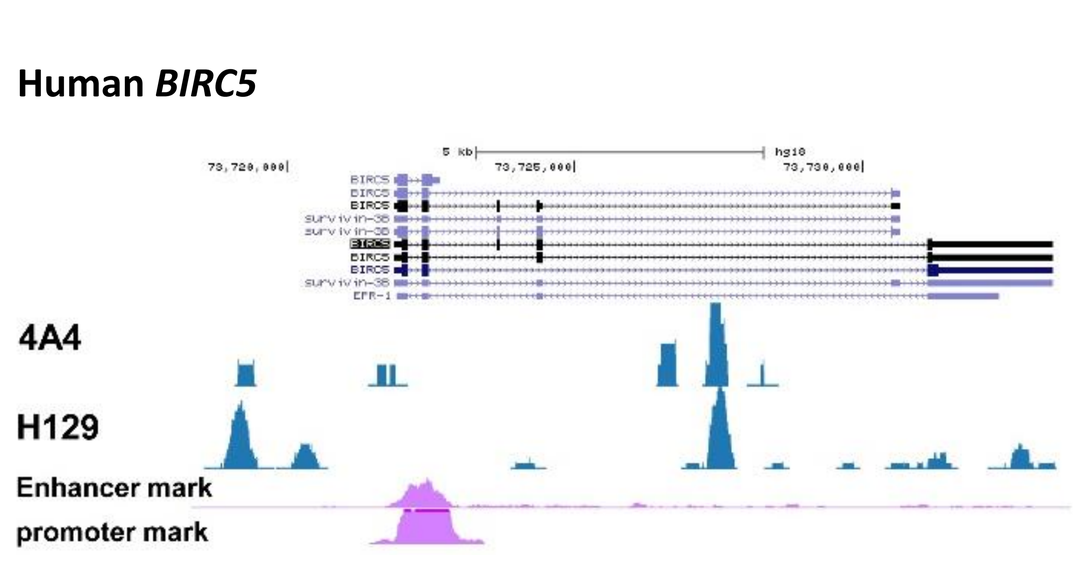
g
Human BIRC5
4A4
H129
Enhancer mark
promoter mark

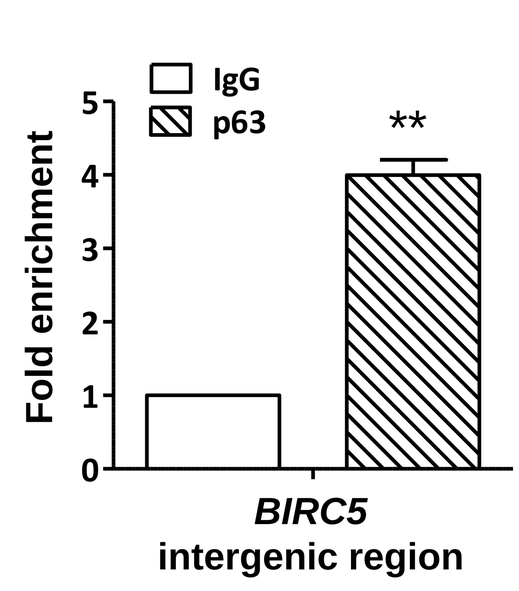
h
IgG
p63
Fold enrichment
5
4
3
2
1
0
**
BIRC5
intergenic region

Fig. 5

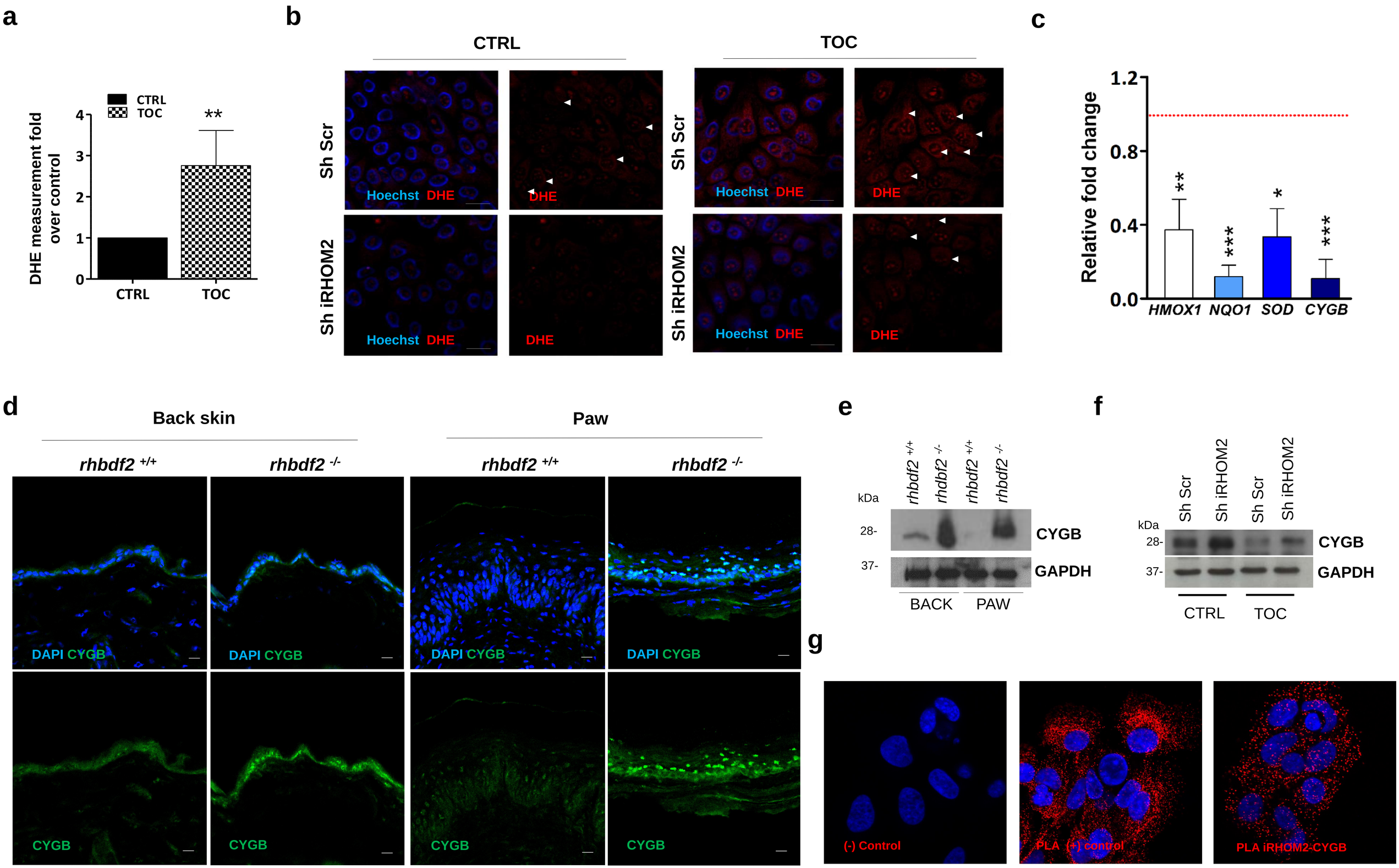
a
CTRL
TOC
DHE measurement fold over control
0
1
2
3
4
**
CTRL
TOC
b
CTRL
TOC
Sh Scr
Sh iRHOM2
Hoechst DHE
DHE
c
Relative fold change
0.0
0.4
0.8
1.2
**
***
*
***
HMOX1
NQO1
SOD
CYGB
d
Back skin
Paw
rhbdf2 +/+
rhbdf2 -/-
DAPI CYGB
CYGB
e
kDa
28-
37-
CYGB
GAPDH
BACK
PAW
f
Sh Scr
Sh iRHOM2
CTRL
TOC
g
(-) Control
PLA (+) control
PLA iRHOM2-CYGB

Fig. 6

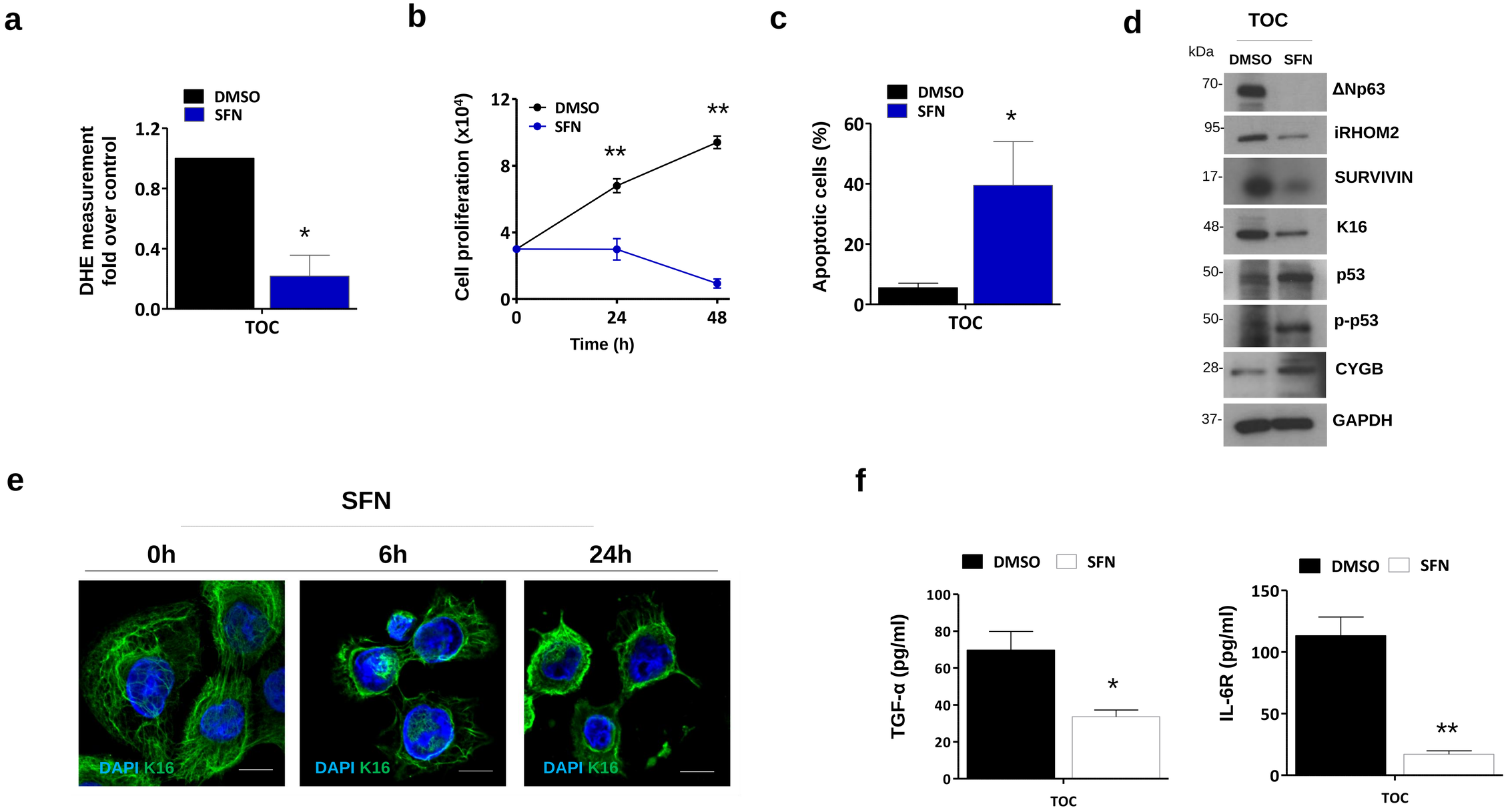
a
DMSO
SFN
DHE measurement fold over control
1.2
0.8
0.4
0.0
*
TOC
b
DMSO
SFN
Cell proliferation (x10⁴)
12
8
4
0
**
**
0
24
48
Time (h)
c
DMSO
SFN
Apoptotic cells (%)
60
40
20
0
*
TOC
d
TOC
kDa
DMSO
SFN
70-
ΔNp63
95-
iRHOM2
17-
SURVIVIN
48-
K16
50-
p53
50-
p-p53
28-
CYGB
37-
GAPDH
e
SFN
0h
6h
24h
DAPI K16
DAPI K16
DAPI K16
f
DMSO
SFN
TGF-α (pg/ml)
100
80
60
40
20
0
*
TOC
DMSO
SFN
IL-6R (pg/ml)
150
100
50
0
**
TOC

Fig. 7

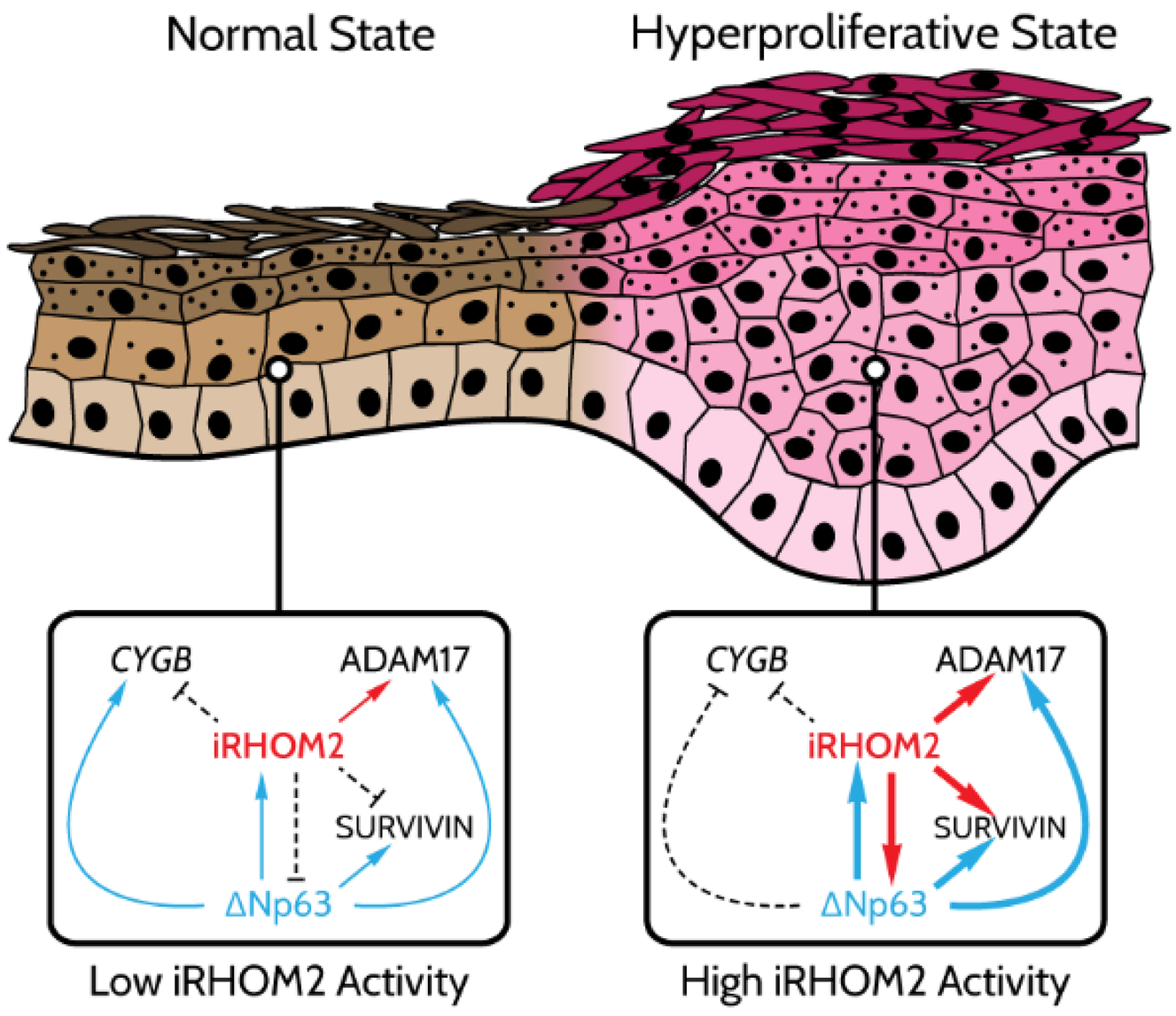
Normal State
Hyperproliferative State
CYGB
ADAM17
iRHOM2
SURVIVIN
ΔNp63
Low iRHOM2 Activity
CYGB
ADAM17
iRHOM2
SURVIVIN
ΔNp63
High iRHOM2 Activity